

# Discovery and development of small-molecule inhibitors of glycogen synthase

*Buyun Tang<sup>1</sup>, Mykhaylo S. Frasinuk<sup>2,3</sup>, Vimbai M. Chikwana<sup>1</sup>, Krishna K. Mahalingan<sup>1</sup>, Cynthia A. Morgan<sup>1</sup>, Dyann M. Segvich<sup>1</sup>, Svitlana P. Bondarenko<sup>3</sup>, Galyna P. Mrug<sup>2,3</sup>, Przemyslaw Wyrebek<sup>4</sup>, David S. Watt<sup>4,6</sup>, Anna A. DePaoli-Roach<sup>1</sup>, Peter J. Roach<sup>1</sup> and Thomas D. Hurley<sup>1\*</sup>*

<sup>1</sup>Department of Biochemistry and Molecular Biology, Indiana University School of Medicine, Indianapolis, Indiana 46202, United States; <sup>2</sup>V. P. Kukhar Institute of Bioorganic Chemistry and Petrochemistry, NAS of Ukraine, Kyiv 02094, Ukraine; <sup>3</sup>National University of Food Technologies, Kyiv 01601, Ukraine; <sup>4</sup>Department of Molecular and Cellular Biochemistry, University of Kentucky, Lexington, Kentucky 40506, United States; <sup>5</sup>Center for Pharmaceutical Research and Innovation, College of Pharmacy, University of Kentucky, Lexington, Kentucky 40536, United States; <sup>6</sup>Lucille Parker Markey Cancer Center, University of Kentucky, Lexington, Kentucky 40536, United States

---

This is the author's manuscript of the article published in final edited form as:

Tang, B., Frasinuk, M. S., Chikwana, V. M., Mahalingan, K. K., Morgan, C. A., Segvich, D. M., Bondarenko, S. P., Mrug, G. P., Wyrebek, P., Watt, D. S., DePaoli-Roach, A. A., Roach, P. J., & Hurley, T. D. (2020). Discovery and Development of Small-Molecule Inhibitors of Glycogen Synthase. *Journal of Medicinal Chemistry*, 63(7), 3538–3551. <https://doi.org/10.1021/acs.jmedchem.9b01851>

**ABSTRACT**

The over-accumulation of glycogen appears as a hallmark in various glycogen storage diseases (GSDs), including Pompe, Cori, Andersen and Lafora disease. Accumulating evidence suggests that suppression of glycogen accumulation represents a potential therapeutic approach for treating these GSDs. Using a fluorescence polarization assay designed to screen for inhibitors of the key glycogen synthetic enzyme, glycogen synthase (GS), we identified a substituted imidazole, (*rac*)-2-methoxy-4-(1-(2-(1-methylpyrrolidin-2-yl)ethyl)-4-phenyl-1*H*-imidazol-5-yl)phenol (**H23**), as a first-in-class inhibitor for yeast glycogen synthase 2 (yGsy2p). Data from X-ray crystallography at 2.85 Å, as well as kinetic data, revealed that **H23** bound within the UDP-glucose binding pocket of yGsy2p. The high conservation of residues between human and yeast GS in direct contact with **H23** informed the development of around 500 **H23** analogs. These analogs produced a structure-activity relationship (SAR) profile that led to the identification of a substituted pyrazole, 4-(4-(4-hydroxyphenyl)-3-(trifluoromethyl)-1*H*-pyrazol-5-yl)pyrogallol, with 300-fold improved potency against human GS. These substituted pyrazoles possess a promising scaffold for drug development efforts targeting GS activity in GSDs associated with excess glycogen accumulation.

## INTRODUCTION

Glycogen is a branched polymer of glucose, composed of chains thirteen residues long on average, arranged in layers to form a molecule of up  $10^7$  daltons, corresponding to 55,000 glucose units. The biosynthesis of glycogen is a highly conserved, complex and coordinated process that involves two key events. Glycogen synthase (GS) lengthens linear chains through the progressive addition of  $\alpha$ -1,4-linked glucose residues to the non-reducing end of the polymer, and glycogen-branching enzyme (GBE) catalyzes the intramolecular transfer of seven glucose residues from the end of a linear chain to a C-6 hydroxyl group to produce  $\alpha$ -1,6 branch points for further elongation<sup>1,2,3,4</sup>.

GS is the rate-limiting enzyme for glycogen biosynthesis<sup>5</sup>. Higher eukaryotes have two isoforms, *GYS1* and *GYS2*<sup>6,7</sup>, that share approximately 70% sequence identity at the amino acid level and display the greatest variation within the N- and C-terminal sequence extensions where regulatory sites are located. The two GS isoenzymes are differentially expressed: *GYS2* is exclusively expressed in the liver, while expression of *GYS1* is highest in skeletal muscle but is also expressed in most other tissues. These two principal storage tissues for glycogen serve distinct physiological roles. Glycogen in the liver plays an essential, regulatory role in glucose homeostasis, but glycogen in other tissues acts as an intracellular energy reserve such as during muscle contraction<sup>8</sup>. Similar to higher eukaryotes, *Saccharomyces cerevisiae* has two genes encoding GS, *GSY1* and *GSY2*, with Gsy2p as the predominant isoform<sup>9</sup>. GS undergoes activation allosterically through glucose-6-phosphate (G6P) binding and inactivation by phosphorylation at a number of sites through the action of multiple protein kinases, including glycogen synthase kinase-3 (GSK-3) in mammals<sup>10,11</sup>. After transport into cells, glucose undergoes phosphorylation to G6P and enters one of several metabolic pathways. Increased

1  
2  
3 levels of intracellular G6P stimulates GS activity that in turn drives the incorporation of glucose  
4 into glycogen in a feed-forward mechanism<sup>12</sup>. The dephosphorylation of GS is mediated by  
5 forms of type 1 protein phosphatase (PP1), the catalytic subunit of which is held in close  
6 proximity to the glycogen granule and GS by a family of glycogen targeting subunits, including  
7 protein-targeting-to-glycogen (PTG), an indirect activator of GS<sup>13</sup>.

8  
9  
10 Glycogen metabolism constitutes a key pathway in living cells that regulates systemic carbon or  
11 energy allocation<sup>14</sup>. A number of diseases are associated with abnormal glycogen metabolism  
12 including type 2 diabetes (T2D) and glycogen storage diseases (GSDs)<sup>15,16,17</sup>. Defects in  
13 enzymes directly involved in either glycogen synthesis or degradation<sup>18</sup> are the basis for more  
14 than 12 different GSDs, and glycogen over-accumulation is characteristic of most GSDs. In  
15 Pompe disease (GSD2), a deficiency of the enzyme, acid- $\alpha$ -glucosidase (GAA), leads to  
16 lysosomal glycogen accumulation in many tissues including skeletal, cardiac, and smooth  
17 muscle<sup>19</sup>. In Cori disease (GSD3) and Andersen disease (GSD4), defects in the glycogen  
18 debranching enzyme (AGL) and glycogen branching enzyme (GBE1), respectively, result in the  
19 accumulation of glycogen with abnormal structure<sup>20,21</sup>. Lafora disease is a fatal progressive  
20 myoclonus epilepsy accompanied by neurodegeneration for which the presence of abnormal  
21 glycogen inclusions known as Lafora bodies<sup>22</sup> are the hallmark. Lafora bodies consist of poorly  
22 branched, hyperphosphorylated, and insoluble forms of glycogen that occur in neuronal, muscle  
23 and other tissues<sup>23,24,25</sup>. Notably, impaired glycogen metabolism and consequent glycogen  
24 accumulation was also found to be pathological for  $\beta$ -cell dysfunction in T2D<sup>16,17</sup>.

25  
26  
27 A common finding with excess glycogen accumulation is an association with impaired  
28 autophagy and dysregulated mitochondrial metabolism. These derangements often lead to cell  
29 death and early-onset lethal, disease progression in GSD-affected patients<sup>16,26,27</sup>. Currently, there

1  
2  
3 are no effective treatments for GSDs that ameliorate all cellular and organ dysfunction. For  
4  
5 example, in Pompe disease, the administration of a genetically engineered enzyme (*i.e.*, Enzyme  
6  
7 Replacement Therapy, ERT) that rescues the defective GAA in peripheral tissues fails to reverse  
8  
9 the neurological defects. Partial suppression of glycogen synthesis through inhibition of GS  
10  
11 activity represents an alternative, potentially effective strategy for treating various types of GSDs  
12  
13 where ERT may not provide a complete solution. For instance, mouse models of Lafora disease  
14  
15 that lack either of the causative genes, *EPM2A* or *EPM2B*, recapitulate aspects of the patient  
16  
17 phenotype, in that they accumulate polyglucosan bodies and misfolded proteins, display  
18  
19 increased endoplasmic reticulum stress, and show signs of neurodegeneration<sup>23,27</sup>. Such animal  
20  
21 models provided a venue for disrupting either *PTG* or *GYS1* in these *EPM2A*<sup>(-/-)</sup> and *EPM2B*<sup>(-/-)</sup>  
22  
23 knock-out mice as a mechanism for diminishing glycogen accumulation, Lafora body formation  
24  
25 and the associated neurological and epileptic symptoms<sup>27,28,29,30</sup>. Inhibition of GS activity *via*  
26  
27 suppression of mTOR signaling also increases the effectiveness of treatments for Pompe disease  
28  
29 in conjunction with ERT<sup>31</sup>. Moreover, a recent report has shown that GYS2 inhibition with  
30  
31 RNAi prevents liver injury in mouse models of GSDs<sup>32</sup>. Although human clinical characteristics  
32  
33 may vary from animal phenotypes, the availability of mouse models and the appearance of  
34  
35 promising therapeutic approaches suggest the feasibility of using small-molecule interventions to  
36  
37 treat GSDs. We now report efforts to develop small-molecule inhibitors of human GS based on a  
38  
39 multicomponent study involving high-throughput screening (HTS), X-ray crystallography and  
40  
41 extensive SAR development work that led to substituted pyrazoles with low micromolar,  
42  
43 inhibitory IC<sub>50</sub> values against human glycogen synthase 1 (hGYS1).  
44  
45  
46  
47  
48  
49  
50

## 51 RESULTS

### 52 Development of fluorescence polarization assay for HTS

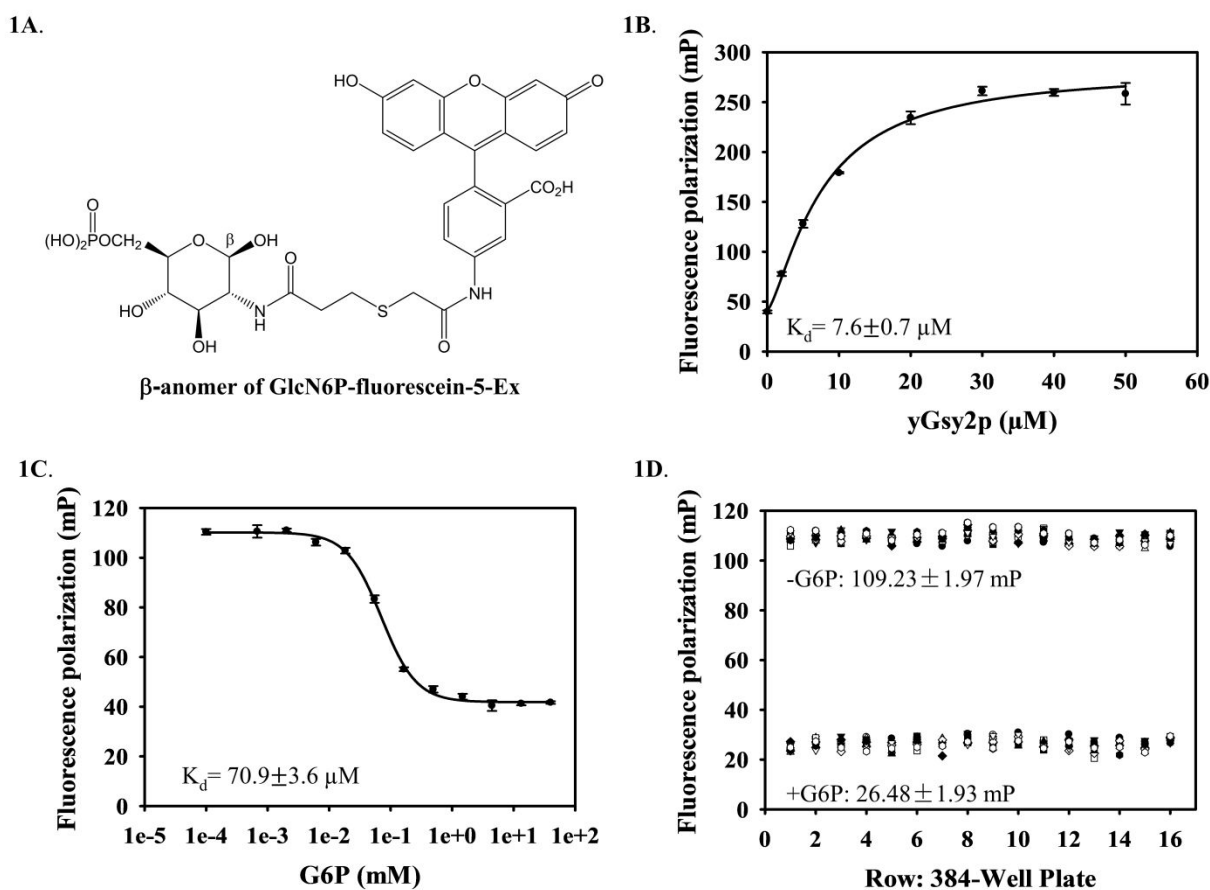
1  
2  
3 The standard radiochemical assay for GS activity utilizes a time-consuming  $^{14}\text{C}$ -glucose  
4 incorporation assay (*i.e.*, UDP-[U- $^{14}\text{C}$ ]glucose and glycogen<sub>(n)</sub> affords [ $^{14}\text{C}$ ]glycogen<sub>(n+1)</sub> and  
5 UDP) that involves appropriate safety measures for handling radioisotopes as well as multiple  
6 transfer and washing steps to remove residual substrates<sup>33</sup>. The combination of laboratory effort,  
7 cost, safety and waste disposal favored the development of a fluorescence polarization (FP) assay  
8 for HTS as a sensitive, inexpensive, and rapid alternative<sup>34</sup>. We reserved the classical  
9 radiochemical assay for subsequent studies to confirm the hits emerging from the FP assay. An  
10 FP assay utilizes a fluorescently-labeled tracer molecule that binds to GS to form a slower  
11 rotating complex than fluorophore alone and that leads to enhanced polarization of the emitted  
12 light. Incubation of the GS-fluorophore complex with small-molecules that displace the  
13 fluorescent tracer produces greater rotational motion of fluorophore than that of the GS-  
14 fluorophore complex and causes relative depolarization of the emitted light. Using this assay  
15 system as a vehicle for HTS, we identified small-molecules that reduce the fluorescence  
16 polarization signal as GS-interacting agents.

17  
18  
19 The development of any FP assay involves the design and synthesis of a functional, fluorescent  
20 probe. Although G6P is a well-known, allosteric activator of GS, the regioselective modification  
21 of similarly reactive hydroxyl groups in G6P presented an unwelcome challenge. Because  
22 glucosamine-6-phosphate (GlcN6P) also activated GS<sup>35</sup> and has a single, reactive amine group,  
23 its selection as a platform on which to incorporate a fluorophore was an attractive alternative to  
24 G6P. Using the  $^{14}\text{C}$ -glucose incorporation assay, we confirmed that either G6P or GlcN6P  
25 activated hGYS1 with  $\text{AC}_{50}$  values of  $1.6 \pm 0.1$  mM or  $5.9 \pm 0.1$  mM, respectively  
26 (**Supplemental Figure 1A**). With direct evidence in hand that GlcN6P activated hGS, we  
27 synthesized a fluorophore-modified GlcN6P (aka GlcN6P-fluorescein-5-Ex) using GlcN6P and

1  
2  
3 the N-hydroxysuccinimidyl ester of fluorescein-5-Ex (**Figure 1A**), purified the fluorophore by  
4 high-performance liquid chromatography (HPLC) and confirmed the expected molecular mass  
5  
6 by mass spectrometry in which it displayed a  $M+H^+$  peak at  $m/z$  735.1267 consistent with  
7  
8  
9  
10  $[C_{31}H_{31}N_2O_{15}PS + H]^+$  with calculated exact mass within acceptable limits (*i.e.*, calculated  $m/z$   
11  
12 735.1256) (**Supplemental Figure 1B**).

13  
14 We examined the binding of the fluorophore, GlcN6P-fluorescein-5-Ex, to GS by adding the  
15  
16 tracer to varying concentrations of yGsy2p to generate a saturation binding curve and calculate a  
17  
18 dissociation constant of  $7.6 \pm 0.7 \mu M$  (**Figure 1B**). Furthermore, a competitive displacement by  
19  
20 G6P ( $K_d = 70.9 \pm 3.6 \mu M$ ) demonstrated that the tracer molecule bound to the G6P allosteric  
21  
22 site (**Figure 1C**). For comparison, we determined yGsy2p activation by G6P using the standard  
23  
24  $^{14}C$ -glucose incorporation assay which yielded an  $AC_{50}$  of  $98.1 \pm 3.1 \mu M$  (**Supplemental**  
25  
26  
27  
28  
29  
30  
31  
32  
33  
34  
35  
36  
37  
38  
39  
40  
41  
42  
43  
44  
45  
46  
47  
48  
49  
50  
51  
52  
53  
54  
55  
56  
57  
58  
59  
60  
**Figure 1C**). We also tested the binding of GlcN6P-fluorescein-5-Ex and displacement by G6P  
using hGYS1. While the GlcN6P-coupled fluorophore and the fluorophore alone bound to  
hGYS1, G6P was unable to displace either compound, a finding that suggested nonspecific  
binding of the fluorophore to hGYS1. This reason, combined with the fact that production of  
human GYS1 in insect cells results in a heavily phosphorylated enzyme that requires very high  
concentrations of G6P for activity measurements, makes the full-length recombinant human  
enzyme unsuitable for an assay designed to displace G6P. However, since the fluorescent probe  
could be fully displaced from yGsy2p through competition with G6P, we used yGsy2p and not  
hGYS1 for HTS. The high conservation of residues within the G6P allosteric site, the active site,  
and overall protein sequence identity (~55%) between yGsy2p and hGYS1 further supported the  
decision to use the yeast enzyme as a screening surrogate for the human enzyme (**Supplemental**  
**Figure 2**). The robustness of the FP assay for HTS was assessed by determining the  $Z'$ -factor, a

parameter reflective of both the signal dynamic range and data variability<sup>36</sup>. While the ideal  $Z'$ -factor is 1, a  $Z'$ -factor between 0.5 and 1 is considered excellent and suitable for screening assays. The FP values for the positive controls (maximal binding, without G6P) and negative controls (fully displaced tracer, with G6P) were  $109.23 \pm 1.97$  and  $26.48 \pm 1.93$  (mean  $\pm$  SD) from the 384-wells, respectively. The  $Z'$ -factor for this assay was determined as 0.86, indicating that this assay is well suited for HTS (Figure 1D).



**Figure 1. Development of fluorescence polarization assay for HTS.** (A) 2-(6-Hydroxy-3-oxo-3H-xanthen-9-yl)-5-(2-((3-oxo-3-(((2R,3R,4R,5S,6R)-2,4,5-trihydroxy-6-(hydroxymethyl)tetrahydro-2H-pyran-3-yl)amino)propyl)thio)acetamido)benzoic acid ( $\beta$ -anomer of GlcN6P-fluorescein-5-Ex). (B) Saturation binding isotherm for GlcN6P-fluorescein-5-Ex



1  
2  
3 binding to yGsy2p. The binding affinity was determined by adding GlcN6P-fluorescein-5-Ex to  
4 a final concentration of 20 nM in the presence of varying yGsy2p concentrations (0 to 50  $\mu$ M).  
5  
6  
7  $K_d = 7.6 \pm 0.7 \mu$ M. Averages of triplicate assays  $\pm$  SEM are shown. (C) Displacement of  
8  
9  
10 GlcN6P-fluorescein-5-Ex binding to yGsy2p by G6P. A mixture of yGsy2p and GlcN6P-  
11  
12 fluorescein-Ex was added to various G6P concentrations (0.68  $\mu$ M to 40 mM).  $K_d = 70.9 \pm 3.6$   
13  
14  $\mu$ M. Averages of triplicate assays  $\pm$  SEM are shown. (D) Z'-factor determination: fluorescence  
15  
16 polarization values of the bound (-G6P), and the free (+2 mM G6P) GlcN6P-fluorescein-5-Ex  
17  
18 are shown, for the 16 rows with each row containing 12 columns of either the bound or free state.  
19  
20  
21 The graphs depict a representative experiment from at least three independent experiments.  
22  
23

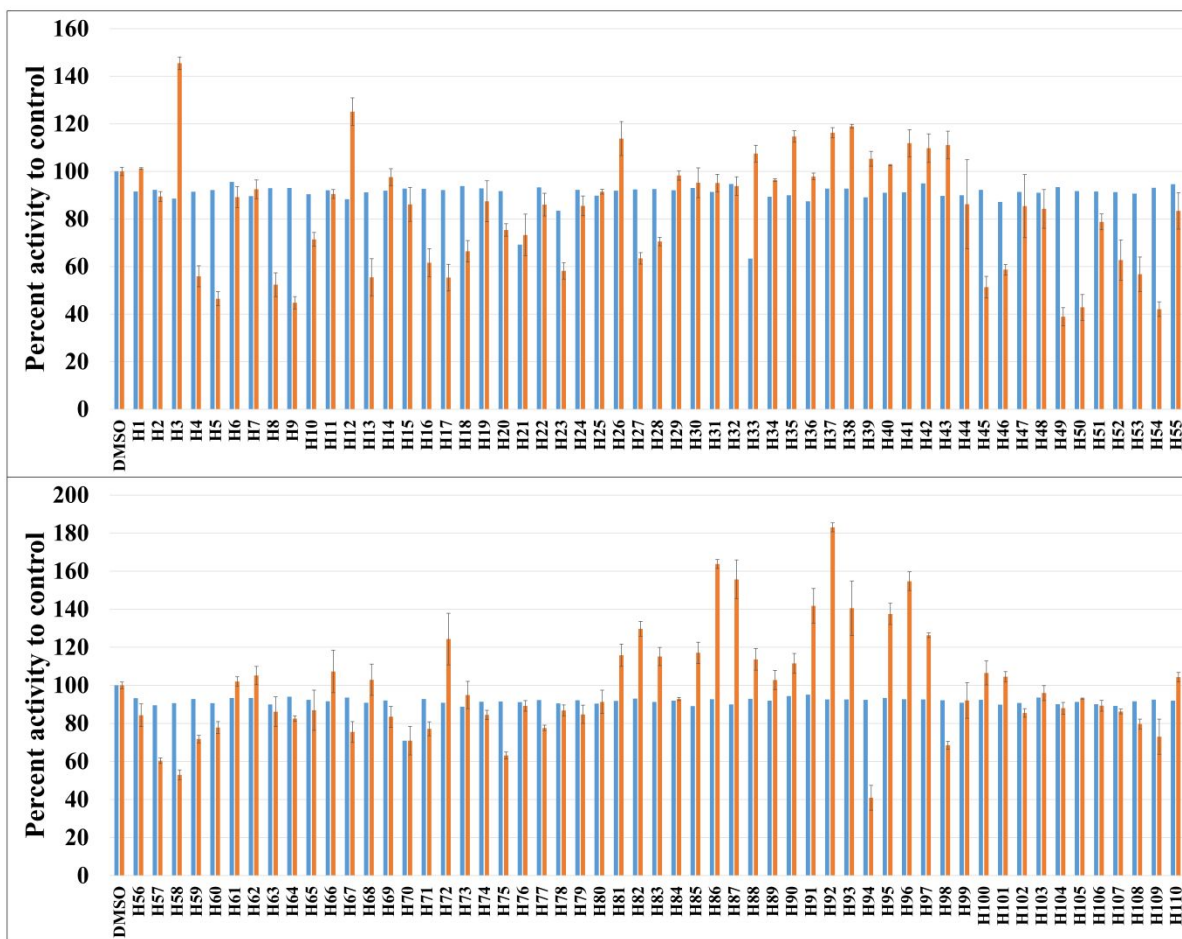
### 24 **Hits identification and validation**

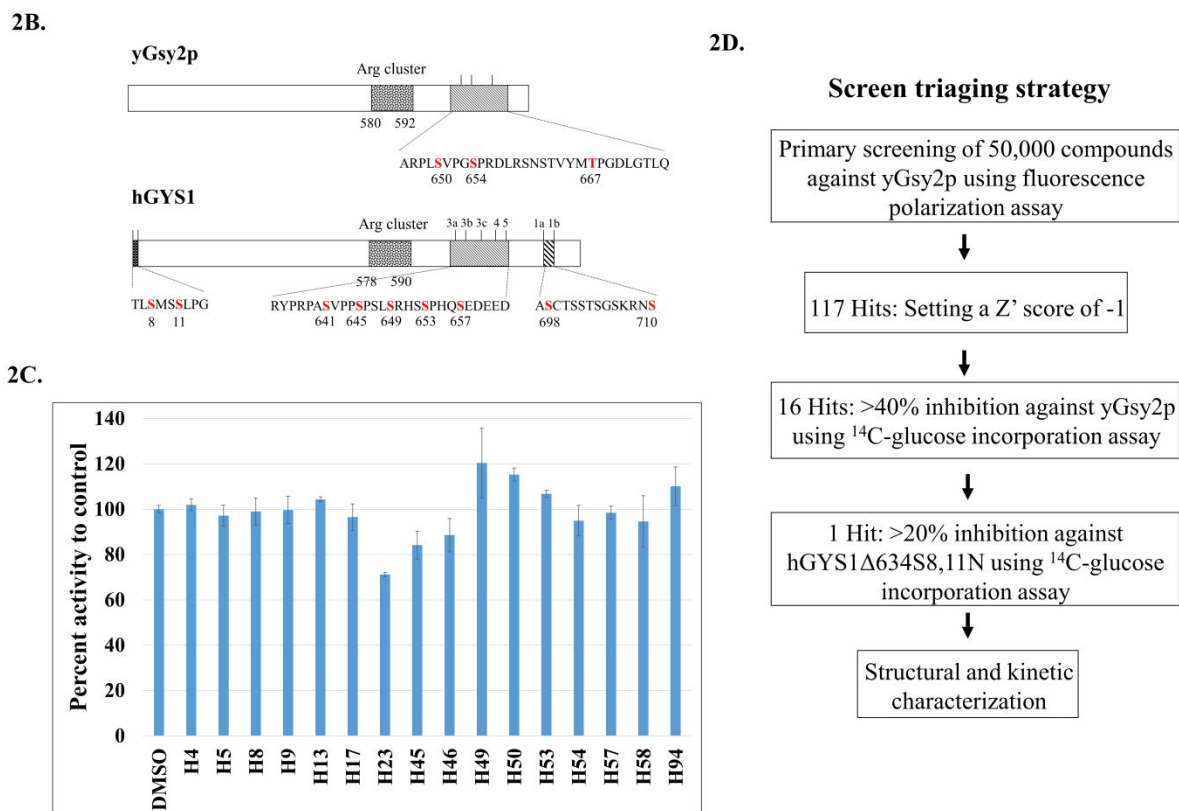
25  
26 We used the aforementioned FP displacement assay to screen the 50K ChemBridge Diversity  
27  
28 library at a final assay concentration of 10  $\mu$ M against the yGsy2p enzyme. The HTS was  
29  
30 adapted to the 384-well plate format using three columns for the DMSO negative controls and  
31  
32 one column for unlabeled G6P as the positive control, resulting in a total of 157 screening plates  
33  
34 **(Supplemental Table 1 and 2)**. We used a Z'-score threshold of -1, corresponding to a  
35  
36 separation of 3 standard deviations between  $\mu_c$  (means of the control DMSO signal) and  $\mu_s$   
37  
38 (means of the library sample signal) as a signal cutoff **(Supplemental Table 2)**. These standards  
39  
40 produced 117 hits and an overall 0.23% hit rate. Initial stock availability led to re-purchasing of  
41  
42 110 compounds (designated **H1-H110**) from ChemBridge and validation of their activity using  
43  
44 the standard  $^{14}$ C-glucose incorporation assay at 100  $\mu$ M concentration. This approach validated  
45  
46 16 hits with greater than 40% inhibition of yGsy2p activity **(Figure 2A)**.  
47  
48  
49

50  
51 Since the yeast yGsy2p enzyme was used as a surrogate for the human hGYS1 enzyme, we next  
52  
53 examined if the 16 validated compounds were also active as inhibitors of hGYS1 activity. To  
54  
55

1  
2  
3 accomplish this necessary confirmation, we redesigned the hGYS1 construct to create a  
4  
5 constitutively active enzyme through deletion of the C-terminal phosphorylation domain  
6  
7 (residues 635-737) and through the substitution of the two N-terminal phosphorylation sites  
8  
9 (Ser8, Ser11) with Asn residues (designated hGYS1 $\Delta$ 634S8,11N) (**Figure 2B**). Purification of  
10  
11 this truncated form of GS in significant quantity led to an enzyme that exhibited an activation  
12  
13 state of  $\sim 0.2$ , a ratio of GS activity in the absence over the presence of G6P as an index of the  
14  
15 phosphorylation state of the enzyme<sup>37</sup>. Unlike the heavily phosphorylated, full-length enzyme  
16  
17 produced in insect cells that had an activation state of  $< 0.01$ <sup>38</sup>, this truncated form of GS was  
18  
19 well suited for validation assays designed to look for inhibitors because the enzyme was neither  
20  
21 overly inhibited by phosphorylation nor rendered insensitive to the effects of G6P. At a test  
22  
23 concentration of 100  $\mu$ M, only 1 hit, namely a substituted imidazole, (*rac*)-2-methoxy-4-(1-(2-  
24  
25 (1-methylpyrrolidin-2-yl)ethyl)-4-phenyl-1*H*-imidazol-5-yl)phenol (**H23**), demonstrated greater  
26  
27  
28  
29  
30  
31 than 20% inhibition using this truncated hGYS1 (**Figure 2C and 2D**).  
32  
33  
34  
35  
36  
37  
38  
39  
40  
41  
42  
43  
44  
45  
46  
47  
48  
49  
50  
51  
52  
53  
54  
55  
56  
57  
58  
59  
60

2A.





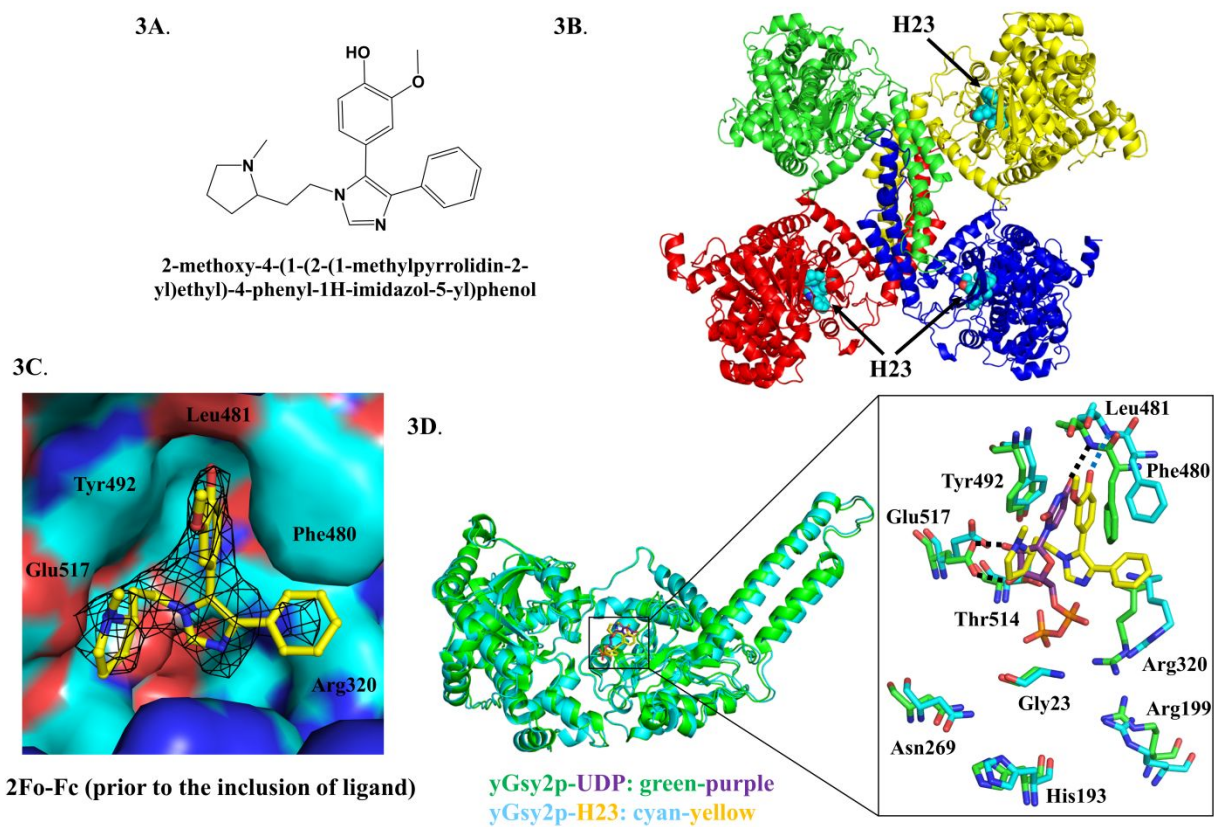
**Figure 2. Hits identification and validation.** (A) In the FP assay, setting a  $Z'$ -score threshold of -1 gave 117 initial hits, out of which 110 (designated **H1-H110**) were re-purchased and tested. The blue column represents the percentage of fluorescence polarization signal to control. The hits were screened at 10  $\mu\text{M}$  in single measurement. The orange column is the percentage of yGsy2p activity to control measured through  $^{14}\text{C}$ -glucose incorporation assay. The hits were tested at 100  $\mu\text{M}$ . Averages of triplicate assays  $\pm$  SEM are shown. (B) Schematic representation of yGsy2p and hGYS1 protein. Phosphorylation residues are shown in red. To generate hGYS1 $\Delta$ 634S8,11N mutant, hGYS1 was truncated at position 634 with mutations of Ser8/11 to Asn to eliminate potential phosphorylation sites. (C) Percentage of hGYS1 $\Delta$ 634S8,11N activity to control measured through  $^{14}\text{C}$ -glucose incorporation assay. The hits were tested at 100  $\mu\text{M}$ . Averages of triplicate assays  $\pm$  SEM are shown. (D) Screening triaging strategy.

### Crystal structure of the H23-yGsy2p complex

Although there are no mammalian GS crystal structures, the structures of two eukaryotic enzymes, namely yGsy2p from *Saccharomyces cerevisiae*<sup>10</sup> and GS from *Caenorhabditis elegans*<sup>39</sup> encouraged our undertaking crystallization experiments. As previously described, yeast Gsy2p existed as tetramer in the crystal structure, and each subunit contained two Rossmann-fold domains with the catalytic site in the interdomain cleft<sup>10</sup>. In the crystal packing environment in crystals of the activated form of GS, one subunit appeared 13.3° more closed than the other three “open” subunits<sup>40</sup>. We successfully determined the crystal structure of the **H23**-yGsy2p complex to a resolution of 2.85 Å (**Table 1**), and we observed **H23** binding in three of the four subunits, all of which corresponded to the “open” domain positions (**Figure 3B**). The structure showed **H23** bound within the active site of GS in a location that overlapped with the binding site for UDP-glucose (UDPG)<sup>40</sup> (**Figure 3C and 3D**). Structural alignment of the R589/592A2·UDP complex to the WT·**H23** complex using their C<sub>α</sub> carbons generated an overall root mean square deviation (rmsd) of 0.36 Å, indicating a high degree of similarity. The binding of **H23** to yGsy2p was mediated by hydrogen-bond formation between the phenolic hydroxyl group of **H23** and the nitrogen backbone of Leu481; hydrophobic interactions of the 2-methoxyphenol sandwiched between Tyr492 and Phe480; van der Waals interactions of the benzene group with the side chains of Phe480 and Arg320; and additional van der Waals interactions of the *N*-methylpyrrolidine moiety with Tyr492, Thr514, and Glu517 (**Figure 3D**).

**Table 1. Structural data and refinement statistics**

Data collection		Refinement	
Space group	<i>I</i> 222	No. reflections	95326
Cell dimensions		$R_{\text{work}}/R_{\text{free}}$	0.20/0.26
a, b, c (Å)	192.3, 206.6, 205.0	r.m.s. deviations	
$\alpha, \beta, \gamma$ (°)	90.0, 90.0, 90.0	Bond lengths (Å)	0.010
Resolution (Å)	50-2.85	Bond angles (°)	1.44
$R_{\text{merge}}$	0.091 (0.766)	Ramachandran plot	
$R_{\text{meas}}$	0.100 (0.843)	Preferred/Allowed (%)	99.01
$R_{\text{pim}}$	0.040 (0.347)	Outliers (%)	0.99
CC1/2	0.999 (0.857)	B-factors	
$I/\sigma(I)$	20.3 (2.0)	Protein	Chain A, 80.1; B, 83.7; C, 91.9; D, 94.6
Completeness (%)	99.7 (100)	Ligand (H23)	Chain A, 100.9; C, 128.3; D, 107.5
Redundancy	6.3 (5.5)		

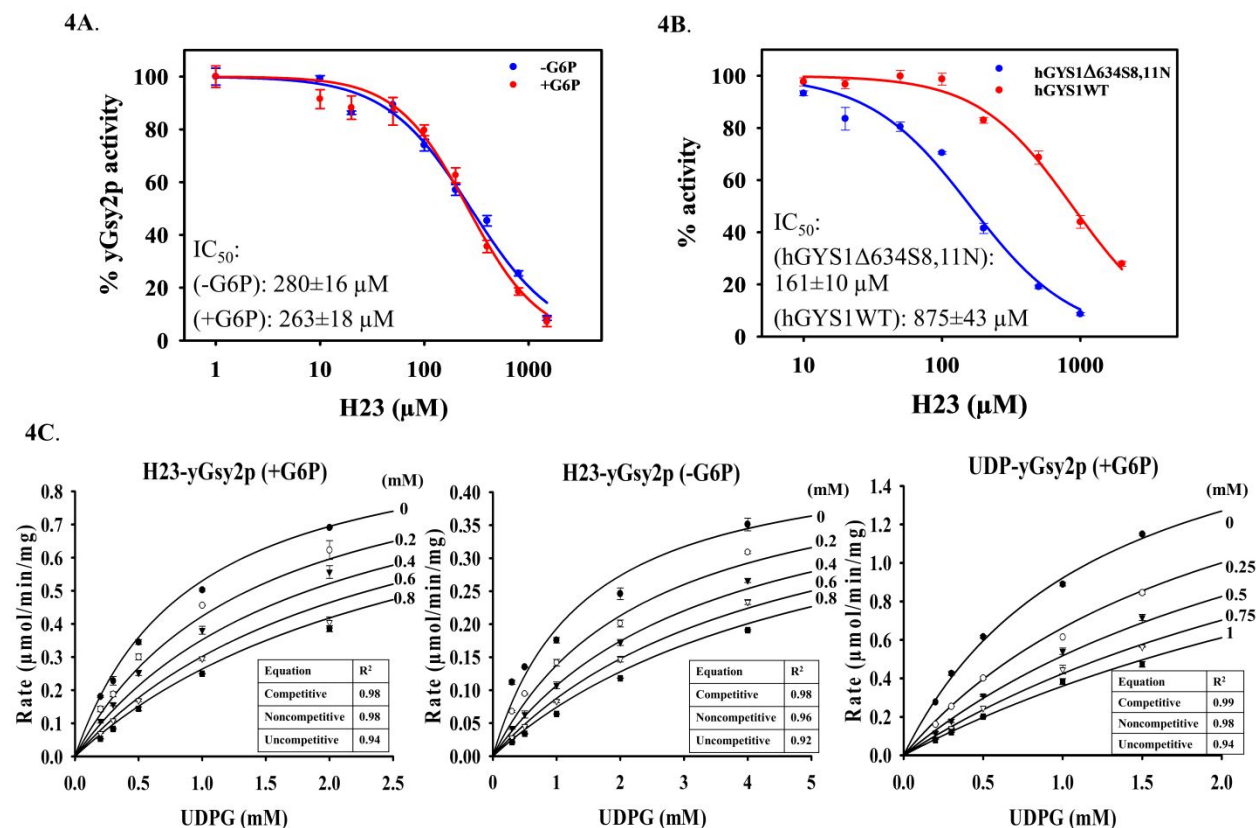


1  
2  
3 **Figure 3. Crystal structure of the H23-yGsy2p complex (PDB: 6U77).** (A) Chemical structure  
4 of **H23**. (B) Ribbon diagram representation of the crystal structure of **H23-yGsy2p** complex.  
5  
6 **H23** is represented by space-filling models in cyan, and binds to three subunits of yGsy2p which  
7 are colored differently. (C) The electron density for **H23** prior to the inclusion of the ligand in  
8 refinement. The map shown is the original unbiased 2Fo-Fc map contoured at 1 standard  
9 deviation. (D) Stick representation of the superposed UDP (purple) and **H23** (yellow) structures  
10 and their interactions with the surrounding amino acids.  
11  
12  
13  
14  
15  
16  
17  
18

### 19 **Kinetic characterization of H23**

20  
21 In a study of the inhibitory potential for **H23** against yeast and human GS using the standard <sup>14</sup>C-  
22 glucose incorporation assay, **H23** exhibited IC<sub>50</sub> values of 280 μM and 263 μM in the absence  
23 and presence, respectively, of G6P for yGsy2p (**Figure 4A**). The similarity in IC<sub>50</sub> values  
24 indicated **H23** was not in direct competition with G6P. Under subsaturating G6P concentrations,  
25 the IC<sub>50</sub> values of **H23** against either hGYS1Δ634S8,11N or wild-type hGYS1 were 161 μM and  
26 875 μM, respectively (**Figure 4B**). Even though the presence or absence of G6P did not impact  
27 **H23** potency, the activity state of the human GS enzyme had a five-fold effect on the binding of  
28 **H23**.  
29  
30  
31  
32  
33  
34  
35  
36  
37  
38  
39

40 To understand **H23** mode of inhibition, we performed co-variation experiments by  
41 simultaneously varying the concentrations of UDPG at different fixed concentrations of **H23** and  
42 fitting the kinetic data against the competitive, non-competitive and uncompetitive inhibition  
43 equations. For yGsy2p, the inhibition data with **H23** was consistent with a competitive mode of  
44 inhibition with respect to varied UDPG, with K<sub>i</sub> values of 370 μM in the presence of G6P, and  
45 290 μM in the absence of G6P. UDP displayed a similar competitive mode of inhibition with a  
46 K<sub>i</sub> value of 350 μM (**Figure 4C**).  
47  
48  
49  
50  
51  
52  
53  
54  
55  
56  
57  
58  
59  
60

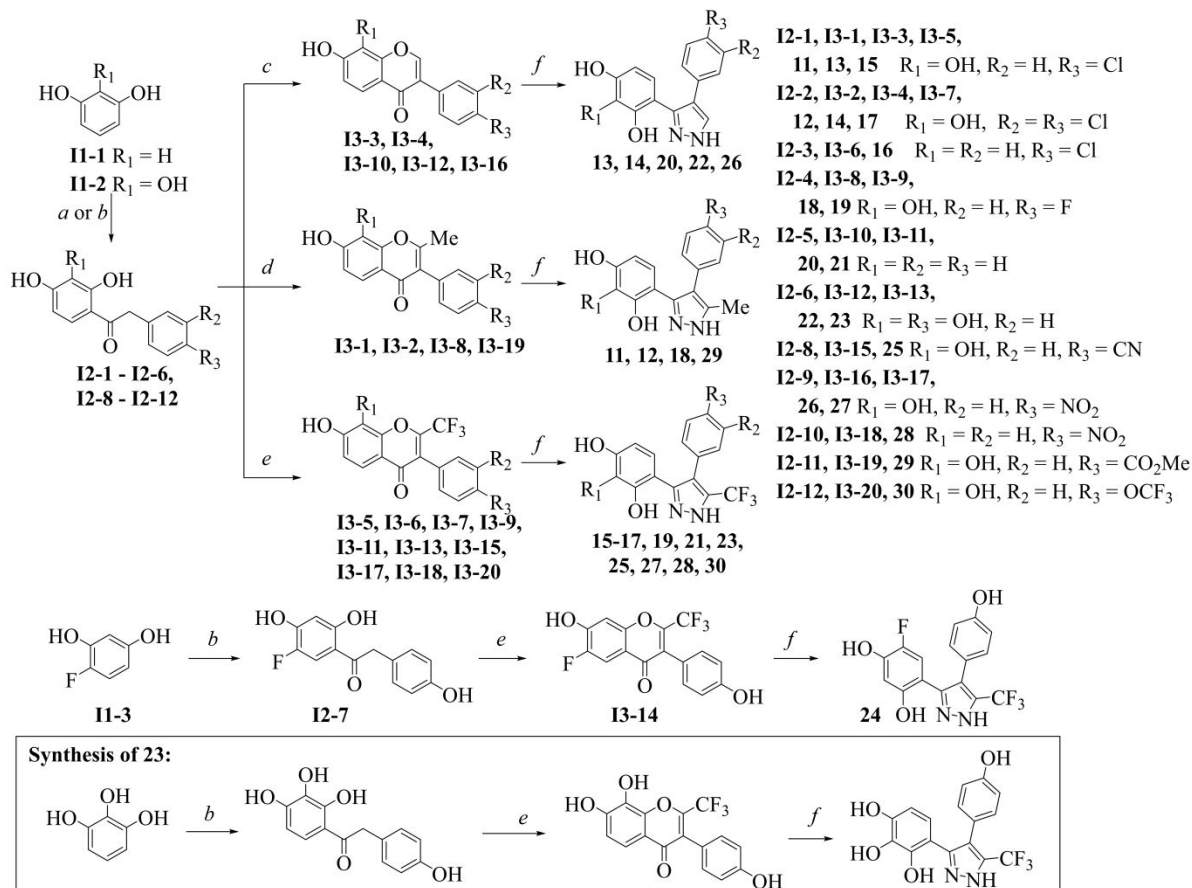


**Figure 4. Kinetic characterization of H23.** (A) Inhibition of H23 to yGsy2p in the absence or presence of G6P. (B) Inhibition of H23 to hGYS1 $\Delta$ 634S8,11N and hGYS1 wild type. All  $\text{IC}_{50}$  curves represent one of three experiments performed using triplicate measurements for each condition, with mean  $\pm$  SEM shown. (C) Michaelis-Menten curves fit to the competitive inhibition equation for varied H23 versus UDPG. The values of goodness of fit ( $R^2$ ) are shown for all equations evaluated. H23 has a  $K_i$  of  $370 \pm 30 \mu\text{M}$  in the presence of G6P and a  $K_i$  of  $290 \pm 20 \mu\text{M}$  in the absence of G6P. UDP is used as a positive control for competitive inhibition against varied UDPG for yGsy2p, which displayed a  $K_i$  of  $350 \pm 10 \mu\text{M}$ . The reported  $K_i$  values are the mean  $\pm$  SEM from three independent experiments in duplicate.



## Development of structure-activity relationships for analogs of H23 toward hGYS1

The overall protein sequence alignment demonstrates 55% sequence identity between yGsy2p and hGYS1. Because the amino acids in the binding site for **H23**, including Arg320, Phe480, Leu481, Tyr492, and Glu517 in yGsy2p, are completely conserved across yeast and human species (**Supplemental Figure 2**), the structural information derived from **H23**-yGsy2p crystal structure provided a useful guide for structure-activity studies focused on hGYS1. We examined a total of 491 analogs that shared at least 50% structural similarity with **H23**, and we tested their activities against yGsy2p, hGYS1 $\Delta$ 634S8,11N, and wild-type hGYS1 using the  $^{14}\text{C}$ -glucose incorporation assay. Our initial kinetic studies showed that a five-membered, heteroaryl (HA) core with a phenyl group at the A<sub>1</sub> position, and a second, vicinal phenyl group were essential elements of **H23** (**Table 2**). Consequently, analog development modified the HA core, A<sub>1</sub> and substructures at R<sub>1</sub>-R<sub>7</sub> positions shown in the structure in **Table 2**. In this study, all **H23** analogs possessed one of the following HA cores: imidazole (designated as HA<sub>1</sub>), pyrrole (designated as HA<sub>2</sub>) or pyrazole (designated as HA<sub>3</sub>). Active compounds appeared in structures with any of these three cores, but the most potent compounds had a pyrazole (HA<sub>3</sub>) scaffold. Commercial libraries were the source of HA<sub>1</sub> and HA<sub>2</sub> compounds in **Table 2**, and a three-step synthesis provided the HA<sub>3</sub> compounds as outlined in **Scheme 1**.



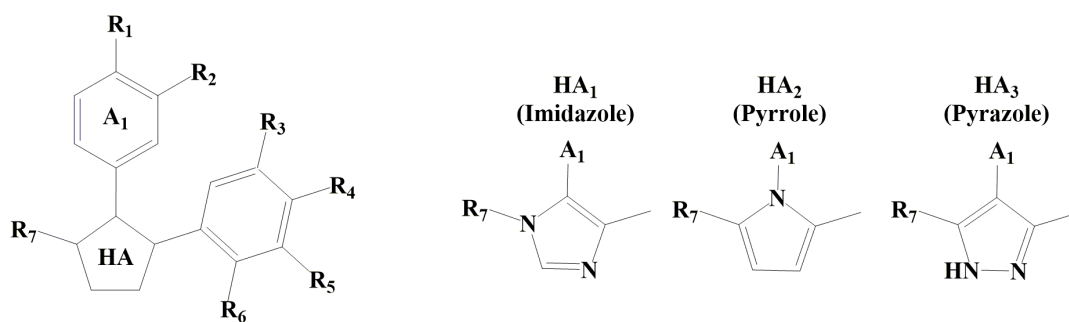
**Scheme 1. Synthesis of pyrazoles 11-30.** Reagents and conditions: (a) (i) arylacetonitrile,  $\text{BF}_3 \cdot \text{Et}_2\text{O}$ ,  $\text{HCl}$  (gas), rt, 6-8 h, (ii)  $\text{H}^+/\text{H}_2\text{O}$ , 0.5-2 h; (b) (i) arylacetic acid,  $\text{BF}_3 \cdot \text{Et}_2\text{O}$ , 80-90 °C, 2 h, (ii)  $\text{H}_2\text{O}$ ; (c) (i)  $\text{DMF}$ ,  $\text{BF}_3 \cdot \text{Et}_2\text{O}$ ,  $\text{POCl}_3$ , 50-60 °C, 2 h, (ii)  $\text{H}_2\text{O}$ ; (d) (i)  $\text{Ac}_2\text{O}$ ,  $\text{KOAc}$ , reflux, 8 h, (ii)  $\text{H}_2\text{SO}_4$ ,  $\text{EtOH}$ , reflux, 0.5 h; (e) (i)  $(\text{CF}_3\text{CO})_2\text{O}$ , pyridine, rt, 48-120 h, (ii)  $\text{H}_2\text{O}$ ; (f)  $\text{N}_2\text{H}_4 \cdot \text{H}_2\text{O}$ , reflux, 0.5-6 h.

A step-by-step program of modifying positions in **H23** involved changes designed either to augment or diminish interactions with substituents in **H23** and the adjoining residues in  $\gamma\text{Gsy}2\text{p}$ . Briefly, starting from the imidazole core (**HA**<sub>1</sub>), we determined that the  $R_1$  hydroxyl group that formed a hydrogen bond with the peptide nitrogen of Leu481 was essential to retain good inhibitory activity (*i.e.*, compare **H23** versus **1** in **Table 2**). The addition of an extra methylene

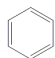
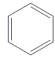
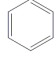
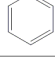
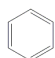
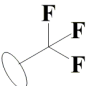
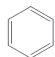
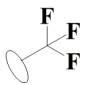
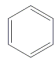
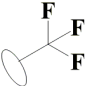
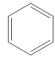
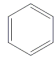
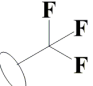
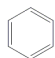
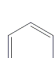
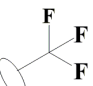
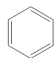
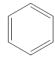
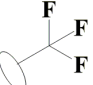
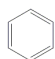
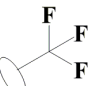
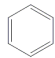

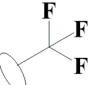
1  
2  
3 unit to the R<sub>7</sub> chain eliminated inhibitory potential (**4** versus **3**). In a similar fashion, the most  
4  
5 potent of the pyrrole HA<sub>2</sub> compounds also had a hydroxyl group at R<sub>1</sub> position (**7** versus **9** or **10**).  
6  
7 Interestingly, substitution of a carboxyl group at R<sub>7</sub> position improved the potency to hGYS1 by  
8  
9 2-fold (IC<sub>50</sub> values for **H23** versus **7**), a finding that suggested different conformational binding  
10  
11 modes for **H23** and **7** for hGYS1.  
12  
13

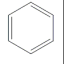
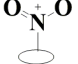
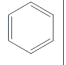
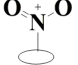
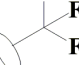
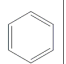
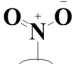
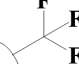
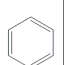
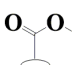
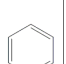
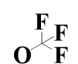
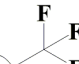
14 Because none of the analogs within the HA<sub>1</sub> or HA<sub>2</sub> series generated noteworthy improvements  
15  
16 in potency, we turned to the pyrazole (HA<sub>3</sub>) series. Within the HA<sub>3</sub> series, SAR studies  
17  
18 demonstrated the importance of a hydrogen bond acceptor at the R<sub>1</sub> position as displayed in the  
19  
20 following order of potency: -OH > -NO<sub>2</sub> > -CN > -F > -H > -Cl (i.e., **23** versus **27**, **25**, **19**, **21** and  
21  
22 **15**). When a chlorine is present at the R<sub>1</sub> position, adding a second chlorine substituent at the R<sub>2</sub>  
23  
24 position improved potency (**12** versus **11** or **14** versus **13** or **17** versus **15**). The most potent  
25  
26 compounds in this series had a pyrogallol group at the R<sub>4-6</sub> positions, and the hydroxyl groups  
27  
28 on this substituent conferred inhibition to GS even if the R<sub>1</sub> position was non-optimal. For  
29  
30 instance, **11** was 16-fold more potent than **H23**. Strikingly, the *meta*-hydroxyl group (R<sub>5</sub>) was  
31  
32 critical to binding. Substitution of this hydroxyl groups with just hydrogen decreased potency  
33  
34 significantly (**16** versus **15** or **28** versus **27**). SAR studies also indicated that substituents at the  
35  
36 R<sub>7</sub> position had an effect on activity in the following order of -CF<sub>3</sub> > -H > -CH<sub>3</sub> (**15** or **13** versus  
37  
38 **11**; **17** or **14** versus **12**). In summary, analog development initiated from the substituted  
39  
40 imidazole **H23** led to a substituted pyrazole, namely 4-(4-(4-hydroxyphenyl)-3-(trifluoromethyl)-  
41  
42 1*H*-pyrazol-5-yl)pyrogallol (**23**) that had an *in vitro* IC<sub>50</sub> value of 2.75 μM, an improvement in  
43  
44 potency toward hGYS1 of more than 300-fold.  
45  
46  
47  
48  
49  
50  
51  
52  
53  
54  
55  
56  
57  
58  
59  
60

Table 2. Structure-activity relationships for H23 analogs



Compound	HA	A <sub>1</sub>	R <sub>1</sub>	R <sub>2</sub>	R <sub>3</sub>	R <sub>4</sub>	R <sub>5</sub>	R <sub>6</sub>	R <sub>7</sub>	%Activity @ 300μM compound			IC <sub>50</sub> (μM)
										yGsy2p	hGYS1Δ 634S8,11N	hGYS1	hGYS1
H23	HA <sub>1</sub>		OH	OCH <sub>3</sub>	H	H	H	H		36.5±0.6	46.5±0.4	77.1±1.2	875±43
1	HA <sub>1</sub>		H	H	H	H	H	H		NI	93.3±1.5	NI	ND
2	HA <sub>1</sub>		H	H	H	H	H	H		72.7±0.4	94.4±2.2	NI	ND
3	HA <sub>1</sub>		OH	H	H	H	H	H		66.6±1.3	56.6±1.3	93.4±2.8	ND
4	HA <sub>1</sub>		OH	H	H	H	H	H		94.8±2.9	NI	NI	ND
5	HA <sub>2</sub>		OH	H	H	H	H	H	CH <sub>3</sub>	79.7±1.0	84.3±0.5	NI	ND
6	HA <sub>2</sub>		OH	H	H	H	H	H		86.0±3.1	NI	NI	ND
7	HA <sub>2</sub>		OH	H	H	H	H	H		40.1±0.9	40.1±0.4	58.9±0.3	384±28
8	HA <sub>2</sub>		OH	H	H	OCH <sub>3</sub>	H	H		34.5±0.4	50.6±3.0	84.0±0.1	ND
9	HA <sub>2</sub>		CONH <sub>2</sub>	H	H	H	H	H		49.3±0.6	40.6±0.1	78.7±0.9	ND
10	HA <sub>2</sub>		F	H	H	H	H	H		84.7±0.1	72.1±4.1	87.5±0.4	ND
11	HA <sub>3</sub>		Cl	H	H	OH	OH	OH	CH <sub>3</sub>	3.52±0.67	6.47±0.09	4.34±0.94	52.9±3.8

Compound	HA	A <sub>1</sub>	R <sub>1</sub>	R <sub>2</sub>	R <sub>3</sub>	R <sub>4</sub>	R <sub>5</sub>	R <sub>6</sub>	R <sub>7</sub>	% Activity @ 20 μM compound			IC <sub>50</sub> (μM)
										yGsy2p	hGYS1Δ 634S8,11N	hGYS1	
11	HA <sub>3</sub>		Cl	H	H	OH	OH	OH	CH <sub>3</sub>	NI	NI	91.8±0.3	52.9±3.8
12	HA <sub>3</sub>		Cl	Cl	H	OH	OH	OH	CH <sub>3</sub>	NI	81.7±2.7	84.7±2.5	ND
13	HA <sub>3</sub>		Cl	H	H	OH	OH	OH	H	NI	79.4±0.9	85.4±0.1	ND
14	HA <sub>3</sub>		Cl	Cl	H	OH	OH	OH	H	76.7±0.5	26.4±2.3	52.5±4.4	19.5±1.3
15	HA <sub>3</sub>		Cl	H	H	OH	OH	OH		51.5±0.4	11.8±2.4	47.5±1.7	19.8±0.5
16	HA <sub>3</sub>		Cl	H	H	OH	H	OH		NI	87.9±1.5	NI	ND
17	HA <sub>3</sub>		Cl	Cl	H	OH	OH	OH		47.4±4.4	5.28±0.16	12.2±1.3	13.7±0.6
18	HA <sub>3</sub>		F	H	H	OH	OH	OH	CH <sub>3</sub>	NI	89.0±1.5	94.0±2.4	ND
19	HA <sub>3</sub>		F	H	H	OH	OH	OH		45.7±12.4	11.7±0.1	47.8±7.0	14.1±0.8
20	HA <sub>3</sub>		H	H	H	OH	OH	OH	H	NI	25.2±1.6	84.7±2.7	ND
21	HA <sub>3</sub>		H	H	H	OH	OH	OH		51.8±1.8	5.68±0.16	47.2±1.2	16.4±0.6
22	HA <sub>3</sub>		OH	H	H	OH	OH	OH	H	6.21±0.59	23.0±1.9	22.6±0.4	9.82±1.06
23	HA <sub>3</sub>		OH	H	H	OH	OH	OH		0.97±0.01	-1.01±0.37	-0.26±0.34	2.75±0.08
24	HA <sub>3</sub>		OH	H	F	OH	H	OH		65.2±2.4	74.2±4.0	78.4±0.9	72.4±6.5
25	HA <sub>3</sub>			H	H	OH	OH	OH		51.2±1.5	8.14±0.65	42.0±1.5	10.1±0.8

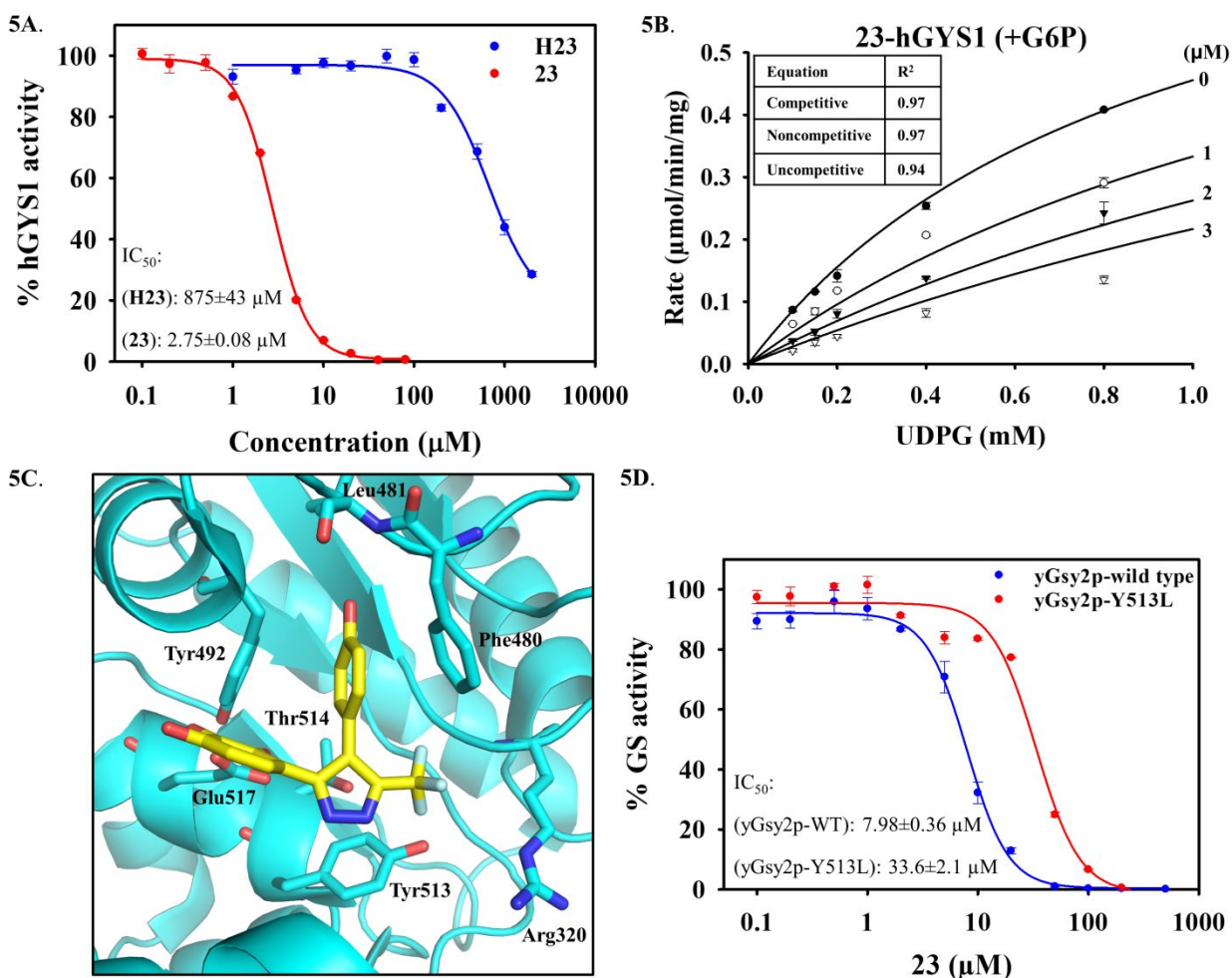
Compound	HA	A <sub>1</sub>	R <sub>1</sub>	R <sub>2</sub>	R <sub>3</sub>	R <sub>4</sub>	R <sub>5</sub>	R <sub>6</sub>	R <sub>7</sub>	% Activity @ 20 μM compound			IC <sub>50</sub> (μM)
										yGsy2p	hGYS1Δ 634S8,11N	hGYS1	hGYS1
26	HA <sub>3</sub>			H	H	OH	OH	OH	H	78.4±5.1	85.0±2.6	66.8±3.7	34.0±7.6
27	HA <sub>3</sub>			H	H	OH	OH	OH		18.8±0.5	10.5±0.1	1.43±0.13	6.54±0.09
28	HA <sub>3</sub>			H	H	OH	H	OH		82.3±7.5	92.7±1.6	89.2±6.4	ND
29	HA <sub>3</sub>			H	H	OH	OH	OH	CH <sub>3</sub>	90.6±5.8	NI	80.1±3.6	ND
30	HA <sub>3</sub>			H	H	OH	OH	OH		91.6±0.6	40.3±2.3	81.4±2.1	ND

For HA<sub>3</sub> Scaffold, IC<sub>50</sub>(S) were determined using a cut-off of 70% activity to hGYS1. Compound 24 is an exception since it has a unique F at R<sub>3</sub> position. NI: no inhibition, greater than 95% activity; ND: not determined. Values are the mean ± SEM from at least three independent experiments in duplicate.

### Kinetic characterization of compound 23

In order to understand the molecular features of our most potent analog, compound **23**, we examined the kinetic characteristics of its interaction with GS (**Figure 5A**). Compound **23** has a competitive mode of inhibition for wild-type hGYS1, with a K<sub>i</sub> value of 1.31 ± 0.14 μM (**Figure 5B**). In light of the SAR and our kinetic results, we hypothesized that the binding of **23** to the active site of yGsy2p resembled the binding of **H23** in the active site. In this model, the hydroxyl group at R<sub>1</sub> position formed a hydrogen bond with the nitrogen backbone of Leu481. The three hydroxyl groups in the pyrogallol subunit formed hydrogen bonds with Thr514 or Glu517. Additional structural flexibility of hydrogen-bond formation depended on the relative position of **23** in the binding pocket. As our SAR study showed, the hydroxyl group at R<sub>5</sub> position was important to confer inhibition, and an additional hydrogen-bond formation between Arg320 and the pyrazole ring may also strengthen binding, particularly when an electron-withdrawing

trifluoromethyl group was present, and diminish binding when electron-donating methyl group was present in the same position in the pyrazole ring (**Figure 5C**). To validate whether compound **23** bound within the active site as modelled, we generated mutation within the active site where Y513 was mutated to L513. This mutation, Y513L, did not abolish GS activity. Unlike other active site mutations that almost completely eliminated enzyme activity, the Y513L mutant decreased GS catalytic activity by only 10-fold. Consistent with our modelled mode of binding, we found that inhibition by **23** toward Y513L was compromised compared to wild type (**Figure 5D**).



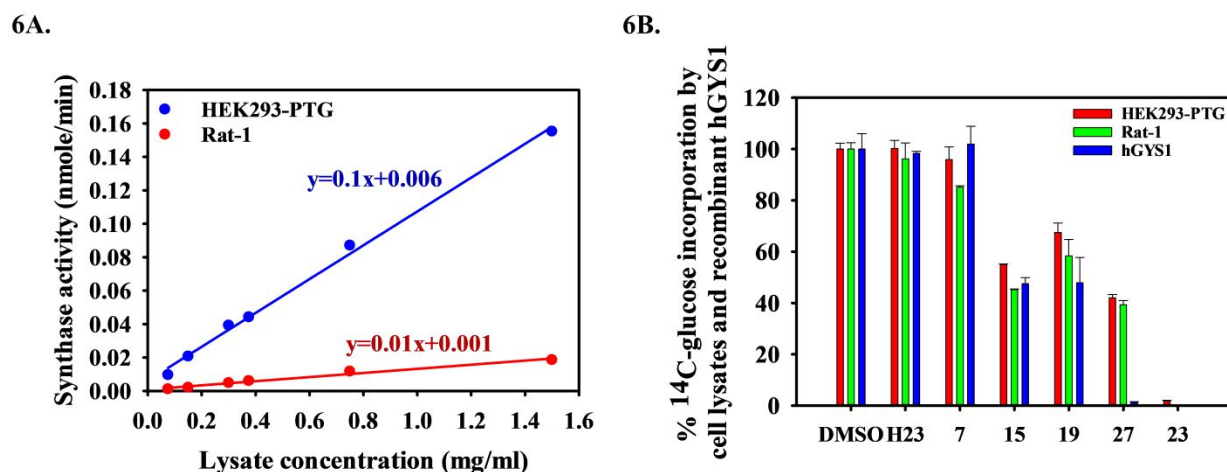
1  
2  
3 **Figure 5. Kinetic characterization of 23.** (A) Dose response curves for parent compound **H23**  
4 and the most potent analog **23** against wild-type hGYS1. (B) Michaelis-Menten curve of  
5  
6 and the most potent analog **23** against wild-type hGYS1. (B) Michaelis-Menten curve of  
7  
8 competitive inhibition for **23** versus UDPG. The values of goodness of fit ( $R^2$ ) are shown for all  
9  
10 equations. **23** shows a  $K_i$  of  $1.31 \pm 0.14 \mu\text{M}$  under the tested condition.  $K_i$  value for **23** is the  
11  
12 mean  $\pm$  SEM from three independent experiments performed using duplicate measurements for  
13  
14 each condition. (C) Hypothetical binding model of **23** to GS in the active site. The hydroxyl  
15  
16 group at  $R_1$  position forms a hydrogen bond with the nitrogen backbone of Leu481. The three  
17  
18 hydroxyl groups flanking the benzene form hydrogen bonds with Tyr514 or Glu517. An  
19  
20 additional hydrogen bond is formed between Arg320 and the pyrazole ring, which is  
21  
22 strengthened when electron-withdrawing group (like  $\text{CF}_3$ ) is present and diminished when  
23  
24 electron-donating group (like  $\text{CH}_3$ ) is present. Manual docking of **23** in the active site was  
25  
26 performed based on SAR and mode of inhibition studies. (D) Validation of **23** binding in the  
27  
28 active site. Compound **23** showed decreased potency against the active-site mutant Y513L  
29  
30 compared with wild-type yGsy2p. All  $\text{IC}_{50}$  curves represent one of three experiments performed  
31  
32 using triplicate measurements for each condition, with mean  $\pm$  SEM shown.

### 33 34 35 36 37 **Inhibition of glycogen synthase activity in cell lysates**

38  
39 We next examined these substituted pyrazoles as inhibitors of GS activity in cell lysates.  
40  
41 Cultured cells normally do not accumulate large amounts of glycogen, largely due to the high  
42  
43 levels of phosphorylation and the resulting low activity state of  $\text{GS}^{26}$ . Lysates from two cell lines  
44  
45 were prepared for GS activity measurement: the HEK293-PTG overexpressing PTG, a regulatory  
46  
47 subunit of protein phosphatase 1, that recruits the phosphatase to glycogen where it promotes the  
48  
49 dephosphorylation and activation of  $\text{GS}^{41,42}$ , and glycogen accumulation; and the Rat-1  
50  
51 fibroblasts which have low GS activity and glycogen as previously described<sup>43,44</sup>. The HEK293-  
52  
53  
54  
55  
56  
57  
58  
59  
60



PTG cells have a seven-fold increase in the GS activity ratio from 0.02 to 0.15. To determine GS activity in lysates and optimize the conditions for measurement, we measured the incorporation of  $^{14}\text{C}$ -glucose into glycogen at 0.2 mM UDPG and 1 mM G6P initially as a function of different lysate concentrations. We observed a linear increase in GS activity within the range of 0.075-1.5 mg/ml lysate. Under the conditions of the assay, the lysate from the HEK293-PTG cells had 10-fold more activity than the Rat-1 cell lysate (**Figure 6A**). To limit substrate utilization to under 10%, we used 0.15 mg/mL HEK293-PTG lysate and 0.75 mg/mL Rat-1 lysate with imidazole **H23**, pyrrole **7** and pyrazoles **15**, **19**, **27** and **23**. When tested at 100  $\mu\text{M}$ , **H23** and **7** did not significantly inhibit GS activity in lysates. However, the remaining four substituted pyrazoles, namely **15**, **19**, **27** and **23**, reduced synthase activity in both HEK293-PTG and Rat-1 cell lysates by >30%. Consistent with its greatest potency toward purified enzyme, pyrazole **23** exhibited almost complete inhibition of synthase activity in lysates (**Figure 6B**). In summary, these analogs targeted GS activity in the context of the glycogen particles present in cellular lysates with potencies similar to those observed in purified enzyme preparations.



**Figure 6. Inhibition of glycogen synthase activity in cell lysates.** (A) Synthase activity in HEK293-PTG and Rat-1 cell lysates in the presence of 0.2 mM UDPG and 1 mM G6P. The data

1  
2  
3 was fit to linear regression line with equations showing synthase activity rate (nmole/min, y-  
4 value) under various lysate concentrations (mg/ml, x-value). The data represent averages of  
5 triplicate assays  $\pm$  SEM. (B) Percent of  $^{14}\text{C}$ -glucose incorporation to control (DMSO) by cell  
6 lysates and recombinant hGYS1 in the presence of **H23** and its analogs. For cell lysates and  
7 recombinant hGYS1, 100  $\mu\text{M}$  and 20  $\mu\text{M}$  compounds were used respectively. Averages of  
8 triplicate assays  $\pm$  SEM are shown.  
9

## 10 11 12 13 14 15 16 17 **DISCUSSION**

18  
19 The suppression of glycogen accumulation emerged as an attractive therapeutic approach for  
20 GSDs whose etiology derived from excessive glycogen storage. Animal models supported this  
21 approach in which genetic or chemical depletion of glycogen alleviated disease symptoms in  
22 models of Lafora disease<sup>27,28,29,30,45</sup>, Pompe disease<sup>31</sup>, and Cori disease<sup>32</sup>. Interestingly, recent  
23 studies suggested that type 2 diabetes (T2D) might also be within the GSD spectrum, as  
24 glycogen accumulation in pancreatic  $\beta$  cells under hyperglycemia contributed to the pathology of  
25  $\beta$ -cell dysfunction<sup>16,17</sup>.  
26  
27  
28  
29  
30  
31  
32  
33  
34

35 Only a few studies identified molecules that targeted glycogen accumulation, including the  
36 widely-used glucose lowering T2D drug metformin<sup>46,47</sup>, mTORC1 inhibitor rapamycin that  
37 indirectly suppress GS activity through signaling regulation<sup>31</sup>, GYS2 RNAi that mediates  
38 enzyme reduction<sup>32</sup>, and the newly developed antibody-enzyme fusion that can degrade  
39 polyglucosan<sup>45</sup>. However, these molecules either targeted glycogen synthesis in an indirect  
40 manner, or present a challenge for the delivery of therapeutics to the central nervous system. In  
41 this study, we adapted a high-throughput fluorescence polarization assay to screen directly for  
42 small-molecule modulators of GS. A HTS of a commercial 50K chemical library identified 117  
43 primary hits against yGsy2p, and through  $^{14}\text{C}$ -glucose incorporation assay only 1 hit was  
44  
45  
46  
47  
48  
49  
50  
51  
52  
53  
54  
55  
56  
57  
58  
59  
60

1  
2  
3 validated as hGYS1 inhibitor (**Figure 2**). The low translation between these two assays might lie  
4  
5 in the nature of these two systems, since fluorescence polarization assay is affinity-based  
6  
7 whereas the radiochemical assay is activity-based. In addition, the kinetic aspects of the two  
8  
9 enzyme systems differ as the impact of regulatory input on the enzyme results in different  
10  
11 outcomes where regulation of yeast GS by G6P primarily impacts  $k_{cat}$ , whereas in mammalian  
12  
13 systems the impact is primarily on  $K_m$  for substrate<sup>48,49</sup>. There is no evidence that the kinetic  
14  
15 steps in catalysis differ between the two enzymes, but it is clear that the manner in which the  
16  
17 rates for those individual steps are impacted by regulatory input does differ. A more sensitive  
18  
19 assay directly targeting hGYS1 is likely to offer better screening outcome. Nonetheless, our FP  
20  
21 assay provided a novel HTS assay as a starting point, and did indeed identify a competitive  
22  
23 inhibitor of UDPG, namely (*rac*)-2-methoxy-4-(1-(2-(1-methylpyrrolidin-2-yl)ethyl)-4-phenyl-  
24  
25 1*H*-imidazol-5-yl)phenol (**H23**), that bound within the active site of yeast yGsy2p. This outcome  
26  
27 was supported by both an X-ray structure and by kinetic studies using **H23** and analogs  
28  
29 developed in a subsequent SAR study. The site of interaction was surprising because the assay  
30  
31 identified small-molecule inhibitors that displaced G6P binding. However, a close inspection of  
32  
33 the known, eukaryotic GS structures demonstrated that the UDPG and G6P binding sites resided  
34  
35 on opposing ends of the same alpha-helix, with Tyr492 stacked against the uracil ring of UDP  
36  
37 and His500 forming a hydrogen bond with the phosphate moiety of G6P (**Supplemental Figure**  
38  
39 **3**). Considering this structural proximity and the cooperative nature of the structural transitions in  
40  
41 GS, it was not surprising that binding at one site could transmit structural information to the  
42  
43 other site and that under the subsaturating conditions of our HTS assay, binding of compounds  
44  
45 within the active site could promote displacement of the fluorophore from the G6P site.  
46  
47  
48  
49  
50  
51  
52  
53  
54  
55  
56  
57  
58  
59  
60

1  
2  
3 Humans have two isoforms of GS, namely hGYS1 and hGYS2. The fact that hGYS1 is  
4  
5 universally expressed in most tissues while hGYS2 is restrictively expressed in liver prompted us  
6  
7 to identify inhibitors against hGYS1 in the hope of diminishing brain glycogen stores, aberrantly  
8  
9 accumulated in some GSDs such as Lafora disease<sup>26</sup>. The high sequence homology between  
10  
11 hGYS1 and hGYS2 enzymes could make it difficult to develop isoform-specific inhibitors.  
12  
13 Nonetheless, inhibition of hGYS2 might aid in the therapeutic efficacy of GSDs with excessive  
14  
15 glycogen accumulation in liver that would ultimately lead to liver damage. Recently, Pursell *et*  
16  
17 *al.* showed that GYS2 inhibition with RNAi prevents liver injury in mouse models of Cori  
18  
19 disease and had no adverse effects<sup>32</sup>.

20  
21  
22 Mutations in GYS1<sup>50</sup> or GYS2<sup>51</sup> in rare GSDs lead to decreased glycogen in muscle and liver  
23  
24 respectively. Disruption of the mouse GYS1 gene resulted in 90% perinatal lethality, likely due  
25  
26 to cardiac developmental problems during embryogenesis, but the surviving mice were  
27  
28 ostensibly normal and lived normal lifetimes<sup>52</sup>. Disruption of GYS2 in mice largely mimicked  
29  
30 the phenotype of human GSD0 patients, namely tendencies to post-prandial hyperglycemia and  
31  
32 to hypoglycemia upon fasting but compatible with a relatively normal life<sup>51,53</sup>. Given that small-  
33  
34 molecule inhibition will not have the penetrance of genetic defects, inhibition of GS activity by  
35  
36 small-molecules is unlikely to elicit extreme phenotypes, and small-molecule inhibition remains  
37  
38 as a potentially valuable means of treating these devastating diseases.

## 39 40 41 42 43 44 45 **CONCLUSIONS**

46  
47 In summary, this study described a strategy for developing a high-throughput FP assay for the  
48  
49 screening of small-molecule inhibitors of GS, the binding mode of a leading imidazole **H23**  
50  
51 validated through both X-ray crystallographic and kinetic data; and an SAR study leading to  
52  
53 analogs, such as pyrazole **23**, with low micromolar potency. These outcomes suggest that  
54  
55

1  
2  
3 targeting glycogen synthase with small-molecule inhibitors represents an attractive approach for  
4  
5 developing new therapeutics for diseases in the GSD family. Unlike other enzyme-based  
6  
7 strategies where complete inhibition is the ultimate objective, a partial reduction of GS activity  
8  
9 may be sufficient to alleviate unwanted and damaging levels of glycogen deposition in the neural  
10  
11 tissue of patients suffering from Lafora disease<sup>27,28,30</sup>. The challenges of developing any  
12  
13 therapeutic, nevertheless, remain the same, and the gulf that stretches between our identification  
14  
15 of a pyrazole inhibitor **23** with activity in the low micromolar range and a therapeutic candidate  
16  
17 is wide and deep. Initial efforts will involve microsomal studies to evaluate anticipated  
18  
19 pharmacokinetic concerns about unwanted redox reactions of pyrazole **23** to 4-(4*H*-pyrazol-4-  
20  
21 ylidene)- or 2,3-dihydroxy-4-(3*H*-pyrazol-3-ylidene)cyclohexa-2,5-dien-1-ones. We will use a  
22  
23 combination of synthesis (*i.e.*, SAR studies) and computational modeling to identify analogs that  
24  
25 avoid this concern and retain desired physiochemical properties (*i.e.*, water solubility;  
26  
27 bioavailability); we will evaluate any promising, new leading structures for potential toxicity  
28  
29 issues (*e.g.*, hERG studies); and we will explore biotinylated analogs to confirm the specificity of  
30  
31 these pyrazole analogs for the desired target. These initial, encouraging results bode well for the  
32  
33 future development of small-molecule strategies to study and potentially treat GSDs.  
34  
35  
36  
37  
38

## 39 40 **EXPERIMENTAL SECTION**

### 41 42 **Materials**

43  
44 The 50K compound Diversity set library, the primary hits **H1-H110**, and analogs **1-4**, **7-9** were  
45  
46 purchased from ChemBridge Corporation (San Diego, CA). Analogs **5**, **6** and **10** were purchased  
47  
48 from Vitas-M Laboratory (Champaign, IL). The purity of these purchased compounds were >  
49  
50 95% based on the spectra (either LC/MS or NMR) provided by the vendors. All pyrazoles were  
51  
52 characterized and validated by both LC/MS and NMR analyses.  
53  
54  
55  
56  
57  
58  
59  
60

### Synthesis and purification of GlcN6P-fluorescein-5-Ex

The tracer was synthesized by using a standard coupling reaction between an amine and N-hydroxysuccinimidyl (NHS) ester. The reaction included: 100 mM NaHCO<sub>3</sub> (pH 8.4), 130 mM glucosamine-6-phosphate (GlcN6P) pH 8.0, 41.6% DMSO and 14 mM fluorescein-Ex, succinimidyl ester. The reaction was incubated for 1 hour at 37°C followed by an overnight incubation at 25°C with continuous stirring, the reaction was stopped by addition of Tris-HCl (pH 8.0) to a final concentration of 0.2 M. Purification of GlcN6P-fluorescein-5-Ex was carried out by HPLC on a semi-preparative Luna C18 column (250×10 mm, 5 μm) from Phenomenex. The eluents used were 25 mM NH<sub>4</sub>OAc (pH 5.5) (E1) and 100% methanol (E2). Elution was performed by the following gradient: T<sub>0</sub>= 5% (v/v) E2, T<sub>10</sub>= 50% (v/v) E2, T<sub>30</sub>= 50% (v/v) E2, T<sub>45</sub>= 75% (v/v) E2, T<sub>55</sub>= 5% (v/v) E2 at a flow rate of 4 mL/min. The fractions containing the UV-containing fractions were collected, dried using a SpeedVac, dissolved in water and stored at -20°C. The fractions containing GlcN6P-fluorescein-5-Ex were identified and confirmed by mass spectrometric analysis. The final tracer concentration was determined by UV spectroscopy (Abs<sub>492</sub>~9.2 × 10<sup>4</sup> M<sup>-1</sup> cm<sup>-1</sup>).

### Fluorescence polarization assay

All the fluorescence polarization (FP) experiments were performed on an EnVision multimode plate reader (Perkin Elmer) with the λ<sub>ex</sub>= 485 nm and λ<sub>em</sub>= 535 nm. The FP experiments were performed in 384-well, black, flat bottom microplates at 25°C. After addition of all reagents, plates were spun down for a minute at 1000g in a centrifuge followed by measurement of the FP signals, where each well was flashed 10 times and the average values were used. All polarization values were expressed as milli-Polarization units (mP), calculated from equation 1:

$$mP = (1000) * \frac{S - G * P}{S + G * P} \quad (1)$$

Where:  $S$ = fluorescence intensity measured when the excitation and emission polarizers are parallel and  $P$ = fluorescence intensity measured when the excitation and emission are perpendicular and  $G$ = grating factor that corrects for instrument bias. All the nonlinear regression analyses were performed by fitting the experimental data to the defined equations using SigmaPlot version 13.0.

### Determination of the GlcN6P-fluorescein-5-Ex/yGsy2p equilibrium dissociation constant

The concentration of the tracer was initially varied from 0-100 nM in order to determine the optimal assay concentration. Based on total fluorescence intensity and mP values, the optimal concentration was determined to lie between 10-40 nM in the final assay. The binding affinity for the tracer for yGsy2p was determined by adding the tracer to a final concentration of 20 nM to each well in the presence of varying yGsy2p concentrations (0 to 50  $\mu$ M) in a final volume of 50  $\mu$ L. The final assay buffer consisted of 15 mM Tris-HCl (pH 7.8) and 15 mM NaCl, the plate was incubated at 25°C for 10 minutes before reading. The dissociation constant, *i.e.*  $K_d$  was calculated by fitting the experimental data to equation 2:

$$f = y_0 + \frac{a * x}{b + x} \quad (2)$$

Where  $f$ =mP,  $y_0$ =mP<sub>min</sub>,  $a$ = mP<sub>max</sub>-mP<sub>min</sub>,  $b$ =  $K_d$  and  $x$ = Concentration of yGsy2p. Experiments were performed in triplicate.

### Activation of yGsy2p or hGYS1 in the presence of G6P or GlcN6P

The activation of hGYS1 or yGsy2p in the presence of G6P or GlcN6P was determined using the radiochemical assay previously described<sup>33</sup> and the data was fit to equation 2. However, the parameters were defined as:  $f$ = % activation,  $y_0$ = % activation<sub>min</sub>,  $a$ =% activation<sub>max</sub> - % activation<sub>min</sub>,  $x$ = Concentration of G6P or GlcN6P and  $b$ = AC<sub>50</sub>. Experiments were performed in triplicate.

### Competitive displacement experiments

G6P was serially diluted in 15 mM Tris-HCl (pH 7.8) to provide a final concentration ranging from 0.68  $\mu$ M to 40 mM. The reaction mixture contained a final concentration of 15 mM Tris-HCl (pH 7.8), 15 mM NaCl, 20 nM GlcN6P-fluorescein-5-Ex, 4.2  $\mu$ M yGsy2p and varying concentrations of G6P in a final volume of 50  $\mu$ L. The plate was incubated for 10 minutes at 25°C before reading. The  $K_d$  was determined by fitting the observed mP changes to equation 3:

$$f1 = mPmin + \frac{(mPmax - mPmin)}{\left(1 + \frac{x}{EC50}\right)^{(-Hillslope)}} \quad (3)$$

Where  $f1 = mP$ ,  $EC_{50} = K_d$ ,  $x =$  Concentration of G6P. Experiments were performed in triplicate.

### Determination of Z'-factor

To determine the quality of the FP-displacement assay for adaptation for HTS, the Z'-factor was calculated using equation 4:

$$Z' = 1 - \frac{3(\sigma_p + \sigma_n)}{|\mu_p - \mu_n|} \quad (4)$$

where  $\sigma_p$  and  $\sigma_n$  are the standard deviations of the signal for the positive and negative controls.

For the negative control 2  $\mu$ L of H<sub>2</sub>O was added and for the positive control 2  $\mu$ L of G6P was added to a final concentration of 2 mM in a 384-well plate. The protein sample was prepared in 25 mM Tris-HCl (pH 7.8), 25 mM NaCl, 7  $\mu$ M yGsy2p, 40 nM tracer and dispensed by a Multi-drop 384 liquid dispenser (Titertek) into the wells with either H<sub>2</sub>O or G6P. The plate was spun down in a centrifuge followed by measurement of the FP signals.

### Expression and purification of yGsy2p and hGYS1

The His-tagged yGsy2p recombinant enzyme was expressed in BL21 (DE3) *Escherichia coli* and purified using a two-step procedure including affinity chromatography on Ni<sup>2+</sup>-nitrilotriacetic acid-agarose and ion exchange purification on Q-sepharose column<sup>10</sup>. The hGYS1 in the pFL



1  
2  
3 vector<sup>38</sup> was modified by deleting the intein-chitin binding domain fusion at the C-terminus and  
4 replacing it with a simple non-cleavable 6 × His-tag at the C-terminus. Purification of the  
5  
6 construct was achieved using Ni-NTA resin (Qiagen product #31314) following manufacturer's  
7  
8 instructions. Separately, a construct of hGYS1 was generated in which the C-terminus was  
9  
10 truncated at position 634 and the N-terminal phosphorylation sites at positions 8 and 11 were  
11  
12 simultaneously mutated to Asn residues, that avoids solubility issues associated with mutation of  
13  
14 these residues to Ala, in order to generate the hGYS1Δ634S8,11N construct. This construct was  
15  
16 also fused to the same C-terminal 6 × His-tag for purification using Ni-NTA resin.  
17  
18  
19  
20  
21

### 22 **Determination of kinetic parameters**

23  
24 Enzyme activity of GS was determined using UDPG as a substrate through <sup>14</sup>C-glucose  
25  
26 incorporation assay by monitoring the amount of radiolabeled glucose being incorporated into  
27  
28 glycogen<sup>33</sup>. Unless otherwise noted, yGsy2p activity was measured in reaction solution  
29  
30 containing 0.3 mM UDPG in the absence or presence of 0.04 mM G6P. The activity of mutant  
31  
32 hGYS1Δ634S8,11N enzyme was measured using 0.2 mM UDPG and 0.4 mM G6P, while the  
33  
34 activity of wild-type hGYS1 was measured using 0.2 mM UDPG and 1 mM G6P. All kinetic  
35  
36 data analyses were performed using the program package SigmaPlot (version 13.0) by fitting the  
37  
38 data to the appropriate kinetic equation. The IC<sub>50</sub> curves for **H23** and its analogs were fit to the  
39  
40 four parameter logistic equation. Titration experiments for Michaelis–Menten curves were  
41  
42 performed by covarying inhibitor and substrate concentrations. The reaction mixture contained 5  
43  
44 μg/ml yGsy2p, varied UDPG (0.2-8 mM in the absence or presence of 7.2 mM G6P) and **H23**  
45  
46 concentrations (0-0.8 mM). All data were fit to competitive, non-competitive and uncompetitive  
47  
48 inhibition models in SigmaPlot (Version 13.0). Appropriate model was selected through analysis  
49  
50 of goodness-of-fit and the residuals of those fits. All experiments include the controls contained  
51  
52  
53  
54  
55  
56

1  
2  
3 2% (v/v) DMSO. The values presented here are the averages  $\pm$  the standard errors of the mean of  
4  
5 three independent experiments with duplicate measurements for each data point in each  
6  
7 experiment.  
8  
9

### 10 **Crystallization and structure determination**

11  
12 Yeast Gsy2p crystals were obtained using hanging drop vapor diffusion method<sup>10</sup>. Briefly, the  
13  
14 protein solution was prepared at 3 mg/ml containing 25 mM G6P. The protein solution was  
15  
16 mixed with crystallization reservoir solution containing 0.1 M Bis-Tris, pH 5.9 and 13-15%  
17  
18 PEG300. The crystals were soaked with compounds (0.5 mM) on sitting drop plates to obtain  
19  
20 inhibitor-bound yGsy2p complex. The crystals were cryo-protected and frozen. Diffraction data  
21  
22 sets were collected using X-ray crystallography at the Advanced Photon Source at beamline 19-  
23  
24 ID, operated by the Structural Biology Center at Argonne National Laboratory. The data sets  
25  
26 were then indexed, integrated and scaled using the HKL3000 program package. The structures  
27  
28 were solved by molecular replacement using MOLREP, as implemented in the Collaborative  
29  
30 Computational Project Number 4 (CCP4) program suite. The G6P bound yGsy2p-R589/592A2  
31  
32 mutant structure (pdb code: 3NB0) was used as the model for molecular replacement. The  
33  
34 structures were initially refined with a single round of rigid body refinement for individual  
35  
36 domains, followed by iterative rounds of restrained refinement with the application of domain-  
37  
38 based TLS and NCS restraints using REFMAC5 as implemented in CCP4. COOT (version  
39  
40 0.7.2.1) was used to visually inspect and manually adjust the refined models.  
41  
42  
43  
44  
45  
46

### 47 **Compound synthesis**

48  
49 Synthesis of pyrazoles **11-30** was performed in a 3-step procedures which include 1) synthesis of  
50  
51 polyhydroxydeoxybenzoins; 2) ring-closure reaction for the synthesis of isoflavones with or  
52  
53 without de-acetylation of phenolic groups; and 3) recyclization reaction of chromones under  
54  
55  
56  
57  
58  
59  
60

1  
2  
3 hydrazine actions (**Scheme 1**). Initial Hoesch reaction of substituted polyphenols and  
4  
5 arylacetonitriles in boron trifluoride etherate with passing of anhydrous HCl led to formation of  
6  
7 A-ring polyhydroxylated deoxybenzoins **I2-1 – I2-5** and **I2-9 – I2-12**<sup>54</sup>. Alternative condensation  
8  
9 of pyrogallol or 4-fluoresorcinol with phenylacetic acids in boron trifluoride etherate at  
10  
11 heating was performed for the synthesis of 4'-hydroxy- or 4'-cyano deoxybenzoins **I2-6 – I2-8**<sup>55</sup>.  
12  
13 Ring-closure reaction with Vilsmeier reagent or trifluoroacetic anhydride in pyridine after work-  
14  
15 up with water afford 2-unsubstituted or 2-trifluoromethyl isoflavones. Synthesis of 2-methyl  
16  
17 isoflavones **I3-1, I3-2, I3-8, and I3-19** was performed by reaction of polyhydroxydeoxybenzoins  
18  
19 with acetic anhydride in presence of potassium acetate with the following deacylation in ethanol  
20  
21 without purification of intermediate acetates. Target pyrazoles **11-30** were synthesized by the  
22  
23 reaction of synthesized 2 (un)substituted isoflavones **I3-1 – I3-20** with hydrazine hydrate in  
24  
25 ethanol under reflux.  
26  
27  
28  
29

### 30 31 **Analysis of GS activity from cell lysates**

32  
33 HEK293-PTG cells were generated by transfecting HEK293 cells<sup>56</sup> with the plasmid pCDH-  
34  
35 FLAG-PTG, harboring the mouse PTG coding region and the hygromycin antibiotic resistance  
36  
37 gene utilizing Lipofectamine following manufacturer specifications. Mixed clones were selected  
38  
39 for ~10 days in the presence of 0.2 mg/mL hygromycin, expanded and stored in liquid N<sub>2</sub>.  
40  
41 Analyses of protein expression, GS activity ratio in the absence and presence of saturating  
42  
43 concentrations of UDPG (4.4 mM) and of G6P (7.2 mM) and glycogen levels indicated that the  
44  
45 protein was expressed, the GS activity ratio was increased 7-fold, from 0.02 in control cells to  
46  
47 0.15 in transfected cells, and that glycogen was increased by 90-fold. Quantitation of the  
48  
49 expression of PTG is difficult because the basal levels are very low, undetectable under our  
50  
51 conditions.  
52  
53  
54  
55  
56  
57  
58  
59  
60

1  
2  
3 For lysate preparation the HEK293-PTG cells were cultured in 100 mm plate with 5.5 mM  
4  $\alpha$ MEM, 10% FBS, 6  $\mu$ g/mL penicillin, 10  $\mu$ g/mL streptomycin, and 0.2 mg/ml hygromycin. Rat-  
5  
6  
7  
8  
9  
10  
11  
12  
13  
14  
15  
16  
17  
18  
19  
20  
21  
22  
23  
24  
25  
26  
27  
28  
29  
30  
31  
32  
33  
34  
35  
36  
37  
38  
39  
40  
41  
42  
43  
44  
45  
46  
47  
48  
49  
50  
51  
52  
53  
54  
55  
56  
57  
58  
59  
60

1 cells were cultured in 100 mm plate with 25 mM DMEM, 10% FBS, 6  $\mu$ g/mL penicillin and 10  $\mu$ g/mL streptomycin. Cells were grown for 3-4 days till confluency. Before harvest, cells were washed twice with 5 mL ice-cold GS buffer (50 mM Tris-HCl pH 7.8, 20 mM EDTA, 25 mM KF). Then 400  $\mu$ L GS homogenization buffer (50 mM Tris-HCl pH 7.8, 10 mM EDTA, 2 mM EGTA, 100 mM NaF) with protease inhibitor (0.1 mM TLCK, 10  $\mu$ g/ml leupeptin, 1 mM benzamidine, 0.5 mM PMSF, 1 mM  $\text{Na}_3\text{VO}_4$ ) and  $\beta$ -mercaptoethanol (0.4%) plus Triton  $\times$  100 (0.2%) were added to each 100 mm plate. Plates were frozen on liquid  $\text{N}_2$  and scraped. Then lysates were transferred to 2 ml Eppendorf tube, sonicated for 15 seconds twice on ice, and placed on nutator for 10 minutes at 4  $^\circ\text{C}$ . Protein concentrations were measured using the Bradford reagent and indicated that the protein concentration was the same in both lysates. GS activity was initially measured with varying concentration of the lysates. For monitoring the effect of small-molecules on GS, HEK293-PTG cell lysates were diluted 10-fold while Rat-1 cell lysates were diluted 2-fold in homogenization buffer to achieve steady-state kinetics under the conditions we used in  $^{14}\text{C}$ -glucose incorporation assay<sup>33</sup>. GS activity in cell lysates was measured in 50 mM Tris-HCl buffer at pH 7.8 with 6.7 mg/ml glycogen, and subsaturating concentrations of UDPG (0.2 mM) and G6P (1 mM) in the absence or presence of 100  $\mu\text{M}$  **H23** and its analogs. All assays including the controls contained 2% (v/v) DMSO.

### Generation of yGsy2p Y513L mutant

To characterize the binding pattern of compound **23**, active site mutation Y513L was made without necessarily compensating enzyme activity. Point mutation of Y513L was performed using QuikChange II Site-Directed Mutagenesis Kit (Agilent Technologies) in the pET-28A

1  
2  
3 harboring the yeast Gsy2p cDNA<sup>49</sup> using forward primer 5'-  
4  
5 CTACGAGCCTTGGGGTCTCACACCTGCAGAATGTAC-3' and its complement primer, and  
6  
7 was confirmed by DNA sequencing. The mutant protein was purified exactly the same way as  
8  
9 was yGsy2p. However, the yield was significantly less compared to WT protein. Additionally,  
10  
11 the activity of Y513L mutant is around 10-fold lower than WT enzyme. Kinetics experiments  
12  
13 with Y513 mutant were performed under saturating G6P concentration (7.2 mM).  
14  
15

## 16 17 **ASSOCIATED CONTENT**

### 18 19 **Supporting Information**

20 Supplemental Figures S1-S3; Supplemental Tables S1-S2; Vendor Supplied Compound Purity;  
21  
22 LC/MS and NMR Confirmation of Author Provided Compound Purity (PDF)  
23  
24  
25  
26  
27 Molecular Formula Strings (CSV)  
28

### 29 30 **Accession Code**

31  
32 The structure-factors and derived atomic coordinates for the complex between **H23** and yeast  
33  
34 Gsy2p have been deposited with the RCSB under the code 6U77. Authors will release the atomic  
35  
36 coordinates and experimental data upon article publication.  
37

## 38 39 **AUTHOR INFORMATION**

### 40 41 **Corresponding Author**

42  
43 Tel: +1 317 278 2008; Email address: thurley@iupui.edu.  
44  
45

### 46 47 **Author Contributions**

48  
49 B.T. conducted most of the experiments and summarized all data. V.M.C. conducted the  
50  
51 fluorescence polarization assay for high-throughput screening. M.S.F., S.P.B., G.P.M., P.W., and  
52  
53 D.S.W. synthesized compounds. K.K.M. assisted with structural characterization. A.A.D.R.  
54  
55

1  
2  
3 designed the expression of the His-tagged hGYS1 proteins and generated the HEK293-PTG  
4  
5 cells. C.A.M. purified recombinant hGYS1 protein. B.T. and T.D.H. formed the concept,  
6  
7 designed experiments, analyzed data, and wrote the draft manuscript. B.T., D.S.W., A.A.D.R.,  
8  
9 P.J.R. and T.D.H. reviewed and revised the manuscript.  
10  
11

12 The authors declare no competing interests.  
13  
14

### 15 **Funding Sources**

16  
17 The work at IUPUI was supported by NIH grants R01-DK079887 (TDH), R01-DK27221 (PJR)  
18  
19 and P01-NS056454 (Project 3, PJR). BT was supported by the DeVault Fellowship of the  
20  
21 Indiana University Diabetes and Obesity Program. The work at UK was supported by the  
22  
23 Organic Synthesis Core under NIH P01 NS097197 (to M. Gentry), NIH P30 CA177558 (to L.  
24  
25 Hersh), the Office of the Dean of the College of Medicine, the Center for Pharmaceutical  
26  
27 Research and Innovation in the College of Pharmacy, and NIH UL1 TR000117 from the  
28  
29 National Institutes of Health for University of Kentucky's Center for Clinical and Translational  
30  
31 Science.  
32  
33  
34  
35

### 36 **Conflict of Interest**

37  
38 Thomas D. Hurley holds significant financial equity in SAJE Pharma, LLC and Maze  
39  
40 Therapeutics. Peter J. Roach and Anna A. DePaoli-Roach hold equities with Maze Therapeutics.  
41  
42 However, none of the work described in this study is based on or supported by either company.  
43  
44 David S. Watt has partial ownership in a private venture, Epionc, Inc., to develop small-molecule  
45  
46 inhibitors for cancer treatment. In accord with University of Kentucky policies, David S. Watt  
47  
48 has disclosed this work to the University of Kentucky's Intellectual Property Committee and  
49  
50 complied with stipulations of the University's Conflict of Interest Oversight Committee.  
51  
52  
53  
54  
55  
56  
57  
58  
59  
60

## ACKNOWLEDGEMENTS

We would like to thank the staff at the Structural Biology Center Beamline 19-ID. Results shown in this report were derived from work performed at Argonne National Laboratory, Structural Biology Center at the Advanced Photon Source. Argonne is operated by UChicago Argonne, LLC, for the U.S. Department of Energy, Office of Biological and Environmental Research under contract DE-AC02-06CH11357. This research used resources of the Advanced Photon Source, a U.S. Department of Energy (DOE) Office of Science User Facility operated for the DOE Office of Science by Argonne National Laboratory under Contract DE-AC02-06CH11357. We also thank Dr. Lifan Zeng and Ms. Erica Woodall in the Chemical Genomics Core Facility for assistance with LC/MS. We also specifically thank Dr. Steven M. Johnson for his valuable discussions and recommendations.

## ABBREVIATIONS USED

GSD: glycogen storage disorder; GS: glycogen synthase; yGsy2: yeast glycogen synthase 2; hGYS1: human glycogen synthase 1; SAR: structure-activity relationship; GlcN6P: glucosamine-6-phosphate; G6P: glucose-6-phosphate; PTG: protein-targeting-to-glycogen; HTS: high-throughput screening; UDPG: Uridine diphosphate glucose; FP: fluorescence polarization.

**REFERENCES:**

1. Roach, P. J. Glycogen and its metabolism. *Curr. Mol. Med.* **2002**, 2, 101-120.
2. Roach, P. J.; Depaoli-Roach, A. A.; Hurley, T. D.; Tagliabracci, V. S. Glycogen and its metabolism: some new developments and old themes. *Biochem. J.* **2012**, 441, 763-787.
3. Melendez, R.; Melendez-Hevia, E.; Canela, E. I. The fractal structure of glycogen: a clever solution to optimize cell metabolism. *Biophys. J.* **1999**, 77, 1327-1332.
4. Prats, C.; Graham, T. E.; Shearer, J. The dynamic life of the glycogen granule. *J. Biol. Chem.* **2018**, 293, 7089-7098.
5. Skurat, A. V.; Peng, H. L.; Chang, H. Y.; Cannon, J. F.; Roach, P. J. Rate-determining steps in the biosynthesis of glycogen in COS cells. *Arch. Biochem. Biophys.* **1996**, 328, 283-288.
6. Browner, M. F.; Nakano, K.; Bang, A. G.; Fletterick, R. J. Human muscle glycogen synthase cDNA sequence: a negatively charged protein with an asymmetric charge distribution. *Proc. Natl. Acad. Sci. U. S. A.* **1989**, 86, 1443-1447.
7. Nuttall, F. Q.; Gannon, M. C.; Bai, G.; Lee, E. Y. Primary structure of human liver glycogen synthase deduced by cDNA cloning. *Arch. Biochem. Biophys.* **1994**, 311, 443-449.
8. Jensen, J.; Rustad, P. I.; Kolnes, A. J.; Lai, Y. C. The role of skeletal muscle glycogen breakdown for regulation of insulin sensitivity by exercise. *Front. Physiol.* **2011**, 2, 112.
9. Farkas, I.; Hardy, T. A.; Goebel, M. G.; Roach, P. J. Two glycogen synthase isoforms in *Saccharomyces cerevisiae* are coded by distinct genes that are differentially controlled. *J. Biol. Chem.* **1991**, 266, 15602-15607.
10. Baskaran, S.; Roach, P. J.; DePaoli-Roach, A. A.; Hurley, T. D. Structural basis for glucose-6-phosphate activation of glycogen synthase. *Proc. Natl. Acad. Sci. U. S. A.* **2010**, 107, 17563-17568.



- 1  
2  
3 11. Mahalingan, K. K.; Baskaran, S.; DePaoli-Roach, A. A.; Roach, P. J.; Hurley, T. D.  
4  
5 Redox switch for the inhibited state of yeast glycogen synthase mimics regulation by  
6  
7 phosphorylation. *Biochemistry* **2017**, *56*, 179-188.  
8  
9  
10 12. Bouskila, M.; Hunter, R. W.; Ibrahim, A. F.; Delattre, L.; Pegg, M.; Van Diepen, J. A.;  
11  
12 Voshol, P. J.; Jensen, J.; Sakamoto, K. Allosteric regulation of glycogen synthase controls  
13  
14 glycogen synthesis in muscle. *Cell Metab.* **2010**, *12*, 456-466.  
15  
16  
17 13. Printen, J. A.; Brady, M. J.; Saltiel, A. R. PTG, a protein phosphatase 1-binding protein  
18  
19 with a role in glycogen metabolism. *Science* **1997**, *275*, 1475-1478.  
20  
21  
22 14. Buschiazzo, A.; Ugalde, J. E.; Guerin, M. E.; Shepard, W.; Ugalde, R. A.; Alzari, P. M.  
23  
24 Crystal structure of glycogen synthase: homologous enzymes catalyze glycogen synthesis and  
25  
26 degradation. *EMBO J.* **2004**, *23*, 3196-3205.  
27  
28  
29 15. Wolfsdorf, J. I.; Weinstein, D. A. Glycogen storage diseases. *Rev. Endocr. Metab.*  
30  
31 *Disord.* **2003**, *4*, 95-102.  
32  
33 16. Brereton, M. F.; Rohm, M.; Shimomura, K.; Holland, C.; Tornovsky-Babeay, S.; Dadon,  
34  
35 D.; Iberl, M.; Chibalina, M. V.; Lee, S.; Glaser, B.; Dor, Y.; Rorsman, P.; Clark, A.; Ashcroft, F.  
36  
37 M. Hyperglycaemia induces metabolic dysfunction and glycogen accumulation in pancreatic  $\beta$ -  
38  
39 cells. *Nat. Commun.* **2016**, *7*, 13496.  
40  
41  
42 17. Ashcroft, F. M.; Rohm, M.; Clark, A.; Brereton, M. F. Is type 2 diabetes a glycogen  
43  
44 storage disease of pancreatic  $\beta$  cells? *Cell Metab.* **2017**, *26*, 17-23.  
45  
46  
47 18. Hicks, J.; Wartchow, E.; Mierau, G. Glycogen storage diseases: a brief review and update  
48  
49 on clinical features, genetic abnormalities, pathologic features, and treatment. *Ultrastruct.*  
50  
51 *Pathol.* **2011**, *35*, 183-196.  
52  
53  
54  
55  
56  
57  
58  
59  
60

- 1  
2  
3 19. Kishnani, P. S.; Steiner, R. D.; Bali, D.; Berger, K.; Byrne, B. J.; Case, L. E.; Crowley, J.  
4 F.; Downs, S.; Howell, R. R.; Kravitz, R. M.; Mackey, J.; Marsden, D.; Martins, A. M.;  
5  
6 Millington, D. S.; Nicolino, M.; O'Grady, G.; Patterson, M. C.; Rapoport, D. M.; Slonim, A.;  
7  
8 Spencer, C. T.; Tifft, C. J.; Watson, M. S. Pompe disease diagnosis and management guideline.  
9  
10 *Genet. Med.* **2006**, 8, 267-288.  
11  
12  
13  
14 20. Sentner, C. P.; Hoogeveen, I. J.; Weinstein, D. A.; Santer, R.; Murphy, E.; McKiernan, P.  
15 J.; Steuerwald, U.; Beauchamp, N. J.; Taybert, J.; Laforet, P.; Petit, F. M.; Hubert, A.; Labrune,  
16 P.; Smit, G. P. A.; Derks, T. G. J. Glycogen storage disease type III: diagnosis, genotype,  
17 management, clinical course and outcome. *J. Inherit. Metab. Dis.* **2016**, 39, 697-704.  
18  
19  
20  
21 21. Ferguson, I. T.; Mahon, M.; Cumming, W. J. An adult case of andersen's disease--type  
22 IV glycogenosis: a clinical, histochemical, ultrastructural and biochemical study. *J. Neurol. Sci.*  
23 **1983**, 60, 337-351.  
24  
25  
26  
27 22. Ortolano, S.; Vieitez, I.; Agis-Balboa, R. C.; Spuch, C. Loss of GABAergic cortical  
28 neurons underlies the neuropathology of Lafora disease. *Mol. Brain* **2014**, 7, 7.  
29  
30  
31 23. Gentry, M. S.; Guinovart, J. J.; Minassian, B. A.; Roach, P. J.; Serratosa, J. M. Lafora  
32 disease offers a unique window into neuronal glycogen metabolism. *J. Biol. Chem.* **2018**, 293,  
33 7117-7125.  
34  
35  
36 24. Ganesh, S.; Puri, R.; Singh, S.; Mittal, S.; Dubey, D. Recent advances in the molecular  
37 basis of Lafora's progressive myoclonus epilepsy. *J. Hum. Genet.* **2006**, 51, 1-8.  
38  
39  
40 25. Roach, P. J. Glycogen phosphorylation and Lafora disease. *Mol. Aspects Med.* **2015**, 46,  
41 78-84.  
42  
43  
44 26. Vilchez, D.; Ros, S.; Cifuentes, D.; Pujadas, L.; Valles, J.; Garcia-Fojeda, B.; Criado-  
45 Garcia, O.; Fernandez-Sanchez, E.; Medrano-Fernandez, I.; Dominguez, J.; Garcia-Rocha, M.;

- 1  
2  
3 Soriano, E.; Rodriguez de Cordoba, S.; Guinovart, J. J. Mechanism suppressing glycogen  
4 synthesis in neurons and its demise in progressive myoclonus epilepsy. *Nat. Neurosci.* **2007**, *10*,  
5  
6 1407-1413.  
7  
8  
9  
10 27. Duran, J.; Gruart, A.; Garcia-Rocha, M.; Delgado-Garcia, J. M.; Guinovart, J. J.  
11  
12 Glycogen accumulation underlies neurodegeneration and autophagy impairment in Lafora  
13 disease. *Hum. Mol. Genet.* **2014**, *23*, 3147-3156.  
14  
15  
16  
17 28. Turnbull, J.; DePaoli-Roach, A. A.; Zhao, X.; Cortez, M. A.; Pencea, N.; Tiberia, E.;  
18  
19 Piliguiian, M.; Roach, P. J.; Wang, P.; Ackerley, C. A.; Minassian, B. A. PTG depletion removes  
20  
21 Lafora bodies and rescues the fatal epilepsy of Lafora disease. *PLoS Genet.* **2011**, *7*, e1002037.  
22  
23  
24 29. Pederson, B. A.; Turnbull, J.; Epp, J. R.; Weaver, S. A.; Zhao, X.; Pencea, N.; Roach, P.  
25  
26 J.; Frankland, P. W.; Ackerley, C. A.; Minassian, B. A. Inhibiting glycogen synthesis prevents  
27  
28 Lafora disease in a mouse model. *Ann. Neurol.* **2013**, *74*, 297-300.  
29  
30  
31 30. Turnbull, J.; Epp, J. R.; Goldsmith, D.; Zhao, X.; Pencea, N.; Wang, P.; Frankland, P.  
32  
33 W.; Ackerley, C. A.; Minassian, B. A. PTG protein depletion rescues malin-deficient Lafora  
34  
35 disease in mouse. *Ann. Neurol.* **2014**, *75*, 442-446.  
36  
37  
38 31. Ashe, K. M.; Taylor, K. M.; Chu, Q.; Meyers, E.; Ellis, A.; Jingozyan, V.; Klinger, K.;  
39  
40 Finn, P. F.; Cooper, C. G.; Chuang, W. L.; Marshall, J.; McPherson, J. M.; Mattaliano, R. J.;  
41  
42 Cheng, S. H.; Scheule, R. K.; Moreland, R. J. Inhibition of glycogen biosynthesis via mTORC1  
43  
44 suppression as an adjunct therapy for Pompe disease. *Mol. Genet. Metab.* **2010**, *100*, 309-315.  
45  
46  
47 32. Pursell, N.; Gierut, J.; Zhou, W.; Dills, M.; Diwanji, R.; Gjorgjieva, M.; Saxena, U.;  
48  
49 Yang, J. S.; Shah, A.; Venkat, N.; Storr, R.; Kim, B.; Wang, W.; Abrams, M.; Raffin, M.;  
50  
51 Mithieux, G.; Rajas, F.; Dudek, H.; Brown, B. D.; Lai, C. Inhibition of glycogen synthase II with  
52  
53  
54  
55  
56  
57  
58  
59  
60

- 1  
2  
3 RNAi prevents liver injury in mouse models of glycogen storage diseases. *Mol. Ther.* **2018**, 26,  
4 1771-1782.  
5  
6  
7  
8 33. Thomas, J. A.; Schlender, K. K.; Larner, J. A rapid filter paper assay for UDPglucose-  
9 glycogen glucosyltransferase, including an improved biosynthesis of UDP-14C-glucose. *Anal.*  
10 *Biochem.* **1968**, 25, 486-499.  
11  
12  
13  
14 34. Lea, W. A.; Simeonov, A. Fluorescence polarization assays in small molecule screening.  
15 *Expert Opin. Drug Discov.* **2011**, 6, 17-32.  
16  
17  
18  
19 35. Brady, M. J.; Kartha, P. M.; Aysola, A. A.; Saltiel, A. R. The role of glucose metabolites  
20 in the activation and translocation of glycogen synthase by insulin in 3T3-L1 adipocytes. *J. Biol.*  
21 *Chem.* **1999**, 274, 27497-27504.  
22  
23  
24  
25  
26 36. Zhang, J. H.; Chung, T. D.; Oldenburg, K. R. A simple statistical parameter for use in  
27 evaluation and validation of high throughput screening assays. *J. Biomol. Screening* **1999**, 4, 67-  
28 73.  
29  
30  
31  
32  
33 37. Roach, R. J.; Larner, J. Covalent phosphorylation in the regulation glycogen synthase  
34 activity. *Mol. Cell Biochem.* **1977**, 15, 179-200.  
35  
36  
37  
38 38. Khanna, M.; Imasaki, T.; Chikwana, V. M.; Perez-Miller, S.; Hunter, G. O.; Mosley, A.;  
39 Takagi, Y.; Hurley, T. D. Expression and purification of functional human glycogen synthase-1  
40 (hGYS1) in insect cells. *Protein Expr. Purif.* **2013**, 90, 78-83.  
41  
42  
43  
44  
45 39. Zeqiraj, E.; Tang, X.; Hunter, R. W.; Garcia-Rocha, M.; Judd, A.; Deak, M.; von  
46 Wilamowitz-Moellendorff, A.; Kurinov, I.; Guinovart, J. J.; Tyers, M.; Sakamoto, K.; Sicheri, F.  
47 Structural basis for the recruitment of glycogen synthase by glycogenin. *Proc. Natl. Acad. Sci. U.*  
48 *S. A.* **2014**, 111, E2831-2840.  
49  
50  
51  
52  
53  
54  
55  
56  
57  
58  
59  
60

- 1  
2  
3 40. Chikwana, V. M.; Khanna, M.; Baskaran, S.; Tagliabracci, V. S.; Contreras, C. J.;  
4  
5 DePaoli-Roach, A.; Roach, P. J.; Hurley, T. D. Structural basis for 2'-phosphate incorporation  
6  
7 into glycogen by glycogen synthase. *Proc. Natl. Acad. Sci. U. S. A.* **2013**, 110, 20976-20981.  
8  
9  
10 41. Berman, H. K.; O'Doherty, R. M.; Anderson, P.; Newgard, C. B. Overexpression of  
11  
12 protein targeting to glycogen (PTG) in rat hepatocytes causes profound activation of glycogen  
13  
14 synthesis independent of normal hormone- and substrate-mediated regulatory mechanisms. *J.*  
15  
16 *Biol. Chem.* **1998**, 273, 26421-26425.  
17  
18  
19 42. Greenberg, C. C.; Meredith, K. N.; Yan, L.; Brady, M. J. Protein targeting to glycogen  
20  
21 overexpression results in the specific enhancement of glycogen storage in 3T3-L1 adipocytes. *J.*  
22  
23 *Biol. Chem.* **2003**, 278, 30835-30842.  
24  
25  
26 43. Crook, E. D.; Daniels, M. C.; Smith, T. M.; McClain, D. A. Regulation of insulin-  
27  
28 stimulated glycogen synthase activity by overexpression of glutamine: fructose-6-phosphate  
29  
30 amidotransferase in rat-1 fibroblasts. *Diabetes* **1993**, 42, 1289-1296.  
31  
32  
33 44. Skurat, A. V.; Dietrich, A. D.; Roach, P. J. Glycogen synthase sensitivity to insulin and  
34  
35 glucose-6-phosphate is mediated by both NH<sub>2</sub>- and COOH-terminal phosphorylation sites.  
36  
37 *Diabetes* **2000**, 49, 1096-1100.  
38  
39  
40 45. Brewer, M. K.; Uittenbogaard, A.; Austin, G. L.; Segvich, D. M.; DePaoli-Roach, A.;  
41  
42 Roach, P. J.; McCarthy, J. J.; Simmons, Z. R.; Brandon, J. A.; Zhou, Z.; Zeller, J.; Young, L. E.  
43  
44 A.; Sun, R. C.; Pauly, J. R.; Aziz, N. M.; Hodges, B. L.; McKnight, T. R.; Armstrong, D. D.;  
45  
46 Gentry, M. S. Targeting pathogenic Lafora bodies in Lafora disease using an antibody-enzyme  
47  
48 fusion. *Cell Metab.* **2019**, 30, 689-705.  
49  
50  
51 46. Otto, M.; Breinholt, J.; Westergaard, N. Metformin inhibits glycogen synthesis and  
52  
53 gluconeogenesis in cultured rat hepatocytes. *Diabetes Obes. Metab.* **2003**, 5, 189-194.  
54  
55  
56  
57  
58  
59  
60

- 1  
2  
3 47. Berthier, A.; Paya, M.; Garcia-Cabrero, A. M.; Ballester, M. I.; Heredia, M.; Serratosa, J.  
4  
5 M.; Sanchez, M. P.; Sanz, P. Pharmacological interventions to ameliorate neuropathological  
6  
7 symptoms in a mouse model of Lafora disease. *Mol. Neurobiol.* **2016**, *53*, 1296-1309.  
8  
9  
10 48. Roach, P. J.; Takeda, Y.; Lerner, J. Rabbit skeletal muscle glycogen synthase. I.  
11  
12 relationship between phosphorylation state and kinetic properties. *J. Biol. Chem.* **1976**, *251*,  
13  
14 1913-1919.  
15  
16  
17 49. Pederson, B. A.; Cheng, C.; Wilson, W. A.; Roach, P. J. Regulation of glycogen synthase  
18  
19 identification of residues involved in regulation by the allosteric ligand glucose-6-P and by  
20  
21 phosphorylation. *J. Biol. Chem.* **2000**, *275*, 27753-27761.  
22  
23  
24 50. Kollberg, G.; Tulinius, M.; Gilljam, T.; Ostman-Smith, I.; Forsander, G.; Jotorp, P.;  
25  
26 Oldfors, A.; Holme, E. Cardiomyopathy and exercise intolerance in muscle glycogen storage  
27  
28 disease 0. *N. Engl. J. Med.* **2007**, *357*, 1507-1514.  
29  
30  
31 51. Orho, M.; Bosshard, N. U.; Buist, N. R.; Gitzelmann, R.; Aynsley-Green, A.; Blumel, P.;  
32  
33 Gannon, M. C.; Nuttall, F. Q.; Groop, L. C. Mutations in the liver glycogen synthase gene in  
34  
35 children with hypoglycemia due to glycogen storage disease type 0. *J. Clin. Invest.* **1998**, *102*,  
36  
37 507-515.  
38  
39  
40 52. Pederson, B. A.; Chen, H.; Schroeder, J. M.; Shou, W.; DePaoli-Roach, A. A.; Roach, P.  
41  
42 J. Abnormal cardiac development in the absence of heart glycogen. *Mol. Cell Biol.* **2004**, *24*,  
43  
44 7179-7187.  
45  
46  
47 53. Irimia, J. M.; Meyer, C. M.; Peper, C. L.; Zhai, L.; Bock, C. B.; Previs, S. F.;  
48  
49 McGuinness, O. P.; DePaoli-Roach, A.; Roach, P. J. Impaired glucose tolerance and  
50  
51 predisposition to the fasted state in liver glycogen synthase knock-out mice. *J. Biol. Chem.* **2010**,  
52  
53 285, 12851-12861.  
54  
55

- 1  
2  
3 54. Otsalyuk, V. M.; Tkachuk, T. M.; Bondarenko, S. P.; Chkhalo, V. V.; Khilya, V. P.  
4  
5 Synthetic analogs of xanthocercin. *Chem. Nat. Compd.* **1998**, 34, 284-288.  
6  
7  
8 55. Wahala, K.; Hase, T. A. Expedient synthesis of polyhydroxyisoflavones. *J. Chem. Soc.,*  
9  
10 *Perkin Trans. I.* **1991**, 3005-3008.  
11  
12 56. Graham, F. L.; Smiley, J.; Russell, W. C.; Nairn, R. Characteristics of a human cell line  
13 transformed by DNA from human adenovirus type 5. *J. Gen. Virol.* **1977**, 36, 59-74.  
14  
15  
16  
17  
18  
19  
20  
21  
22  
23  
24  
25  
26  
27  
28  
29  
30  
31  
32  
33  
34  
35  
36  
37  
38  
39  
40  
41  
42  
43  
44  
45  
46  
47  
48  
49  
50  
51  
52  
53  
54  
55  
56  
57  
58  
59  
60

## TABLE OF CONTENTS GRAPHIC

